SCIENCE CHINA
Physics, Mechanics & Astronomy

•Invited Review•

August 2019 Vol. 62 No. 8: 984701
https://doi.org/10.1007/s11433-018-9357-0

Smoothed particle hydrodynamics (SPH) for modeling fluid-structure interactions

Moubin Liu[1,2,3†*], and Zhilang Zhang[1,2,3†]

[1] *BIC-ESAT, College of Engineering, Peking University, Beijing 100871, China;*
[2] *State Key Laboratory for Turbulence and Complex Systems, Peking University, Beijing 100871, China;*
[3] *Institute of Ocean Research, Peking University, Beijing 100871, China*

Received November 29, 2018; accepted January 18, 2019; published online March 29, 2019

Fluid-structure interaction (FSI) is a class of mechanics-related problems with mutual dependence between the fluid and structure parts and it is observable nearly everywhere, in natural phenomena to many engineering systems. The primary challenges in developing numerical models with conventional grid-based methods are the inherent nonlinearity and time-dependent nature of FSI, together with possible large deformations and moving interfaces. Smoothed particle hydrodynamics (SPH) method is a truly Lagrangian and meshfree particle method that conveniently treats large deformations and naturally captures rapidly moving interfaces and free surfaces. Since its invention, the SPH method has been widely applied to study different problems in engineering and sciences, including FSI problems. This article presents a review of the recent developments in SPH based modeling techniques for solving FSI-related problems. The basic concepts of SPH along with conventional and higher order particle approximation schemes are first introduced. Then, the implementation of FSI in a pure SPH framework and the hybrid approaches of SPH with other grid-based or particle-based methods are discussed. The SPH models of FSI problems with rigid, elastic and flexible structures, with granular materials, and with extremely intensive loadings are demonstrated. Some discussions on several key techniques in SPH including the balance of accuracy, stability and efficiency, the treatment of material interface, the coupling of SPH with other methods, and the particle regularization and adaptive particle resolution are provided as concluding marks.

smoothed particle hydrodynamics (SPH), fluid-structure interaction (FSI), computational fluid dynamics (CFD), computational solid dynamics (CSD)

PACS number(s): 02.70.-c, 46.15.-x, 47.11.-j, 83.50.-v

Citation: M. Liu, and Z. Zhang, Smoothed particle hydrodynamics (SPH) for modeling fluid-structure interactions, Sci. China-Phys. Mech. Astron. **62**, 984701 (2019), https://doi.org/10.1007/s11433-018-9357-0

1 Introduction

1.1 Fluid-structure interaction and the role of computational FSI

Fluid-structure interaction (FSI) is a class of mechanics related problems with mutual dependence between the fluid and structure parts. The structure moves and deforms due to the force applied by the neighboring fluid, whereas the movement and deformation of the structure in turn influence the flow dynamics of the fluid. The interactions lead to the mutual dependence of fluids and structures and this two-way interaction loop continues through multiple cycles, possibly resulting in structural damage and less-than-optimal flow. The solid object interacting with ambient fluids can either be a rigid body, an elastic or plastic or even flexible structure, or

†These authors contributed equally to this work.
*Corresponding author (email: mbliu@pku.edu.cn)

a granular material. As such, diversified FSI problems are observable nearly everywhere in engineering and sciences, and also in nature. Typical FSI examples include water entry (e.g., diving of sportsmen) and water exit (e.g., underwater launch of missiles) [1], marine structures interacting with waves and current [2], high-speed vehicles (e.g., train, aircraft and etc.) with aerodynamic loadings [3], hydraulic fracturing in enhanced oil recovery [4], the migration and variations of cells in blood vessels [5] and many others [6-9].

Investigations of fluid-structure interactions are very important in the design of many engineering systems, e.g., marine structures, aircraft, spacecraft, engines and bridges etc. Failing to consider the FSI effects sometimes may be catastrophic, especially for structures comprising materials susceptible to fatigue and for complex fluid flows with moving boundaries. An infamous example is the collapse of the Tacoma Narrows Bridge in 1940 due to the failure of its aeroelastic design, which is a class of FSI-based systems involving the interactions between the inertial, elastic, and aerodynamic forces that occur when an elastic body is exposed to air [10]. Similarly, the other class of FSI, hydroelasticity, occurs when a solid object is exposed to a liquid. One typical example is the liquid sloshing [11,12], in which liquid oscillations due to the motion of a container impose substantial magnitudes of forces and moments to the container structure and further affect the stability of the container transport system in a highly adverse manner. As such, violent liquid sloshing in an oil or liquefied natural gas (LNG) ship can result in local breakages and global instability to the ship, and may further lead to leakage of oil and capsizing of the ship. Similarly, the sloshing of liquefied fuel inside the fuel tank in an aeronautic or astronautic craft can also disturb or even make normal navigation of the craft breakdown.

FSI problems in general are too complex to solve analytically and theoretical investigations are usually valid for simple cases (linear or weakly nonlinear). Experimental techniques are generally expensive, and sometimes certain physical phenomena related to FSI may not be scaled in a real experimental setup. Owing to the recent advancements in the computational techniques and the availability of efficient computing platforms, more studies on FSI are focused on developing numerical models and carrying out simulations. Researches in the fields of computational fluid dynamics (CFD) and computational structural dynamics (CSD) are still on-going, but the maturity of researches in these fields enables the numerical simulation of fluid-structure interaction. There exist some books and reviews addressing the numerical works on FSI problems. Morand and Ohayon [13] presented some numerical methods for modeling fluid-elastic structure interactions in the fields of hydroelasticity and structural acoustics. Dowell and Hall [14] discussed in detail the nonlinear dynamical modeling of FSI problems with its applications in aerospace engineering. Shyy et al. [15] introduced several numerical methods for moving boundary problems including the finite-volume modeling of FSI. Hou et al. [16] presented a review on the representative numerical methods available for computing FSI problems, and they categorized the selected methods and assessed their accuracy and efficiency.

However, FSI usually involves either weak or strong nonlinearity and the mutual dependence of fluids and structures is a two-way interaction loop, which is generally time-dependent [14,16]. For strong FSI problems, the structure may undergo large deformations in elastic or plastic regimes, or even be damaged. On the other side, the fluid may demonstrate complex flow patterns with rapidly changing free surface or even free surface breakup [9,17]. The inherent nonlinearity and time-dependence together with possible large deformations, moving solid-fluid interfaces and free surfaces present great challenges for numerical modeling of FSI problems. Truly predictive FSI methods are in high demand in industry, research laboratories, medical fields, space exploration, and many other fields.

1.2 Grid-based methods

There are basically two approaches in modeling FSI problems. The first one is usually referred to as the monolithic approach, in which the equations governing the fluid flow and the movement of the structure are solved simultaneously with a single solver. As the coupling technique for a fluid and a structure is implemented at each time step in a single solver, the monolithic approach should be more accurate while it requires an effective algorithm and a corresponding computer program developed for this particular combination in the physical systems. The second one is usually referred to as partitioned approach, in which the equations governing the fluid flow and the movement of the structure are solved separately with two distinct solvers. The partitioned approach facilitates solution of the flow equations and the structural equations with different algorithms which have been developed to handle either flow dynamics or structural mechanics. It is therefore flexible and preserves code modularity because an existing CFD solver and an existing CSD solver can be coupled in this approach. However, as the interaction between fluid and structure is not implemented at each time step in a single solver, the partitioned approach is generally not as accurate as the monolithic approach. Moreover, the coupling algorithms in the partitioned approach usually face problems in achieving robustness and stability.

Currently, most of the existing CFD and CSD solvers are based on grid-based methods such as the finite difference method (FDM) [18-20], the finite volume method (FVM) [21-23] and the finite element method (FEM) [24-26]. When modeling FSI problems, a grid-based CFD solver is usually

coupled with a grid-based CSD solver as a partitioned approach. These grid-based methods have been widely applied to solve the governing ordinary or partial differential equations (PDEs). For a long time, the most widely used technique for solving PDEs defined in problem domains with simple geometries is FDM, while in recent decades the FVM dominates in solving fluid flow problems. FEM plays an essential role for computations in solid mechanics, and it is also often applied to FSI problems, for instance, particulate flows [27-29]. In grid-based methods, a continuum domain is divided into discrete small subdomains by the so-called discretization or meshing process. The individual grid points or nodes are connected together in a pre-defined manner by a topological map, which is termed as elements in FEM, cells in FVM, and grids in FDM. The meshing techniques are developed to set up the relationship between the spatial nodes before solving PDEs. By this way, the governing equations can be converted to a set of algebraic equations with nodal unknowns for the field variables.

Due to the pre-defined mesh, conventional grid-based methods suffer from special difficulties which limit their applications in modeling FSI problems. For Lagrangian grid-based methods in a CSD solver such as FEM, a grid is attached on, moves and deforms with the moving objects. It is very difficult to treat large deformations due to possible mesh entanglement. Special techniques like mesh rezoning are usually required, and these techniques are often tedious and time-consuming, and may even introduce additional inaccuracy into the solution [17,30]. For a CFD solver, it is not easy for the Eulerian grid-based methods such as FDM and FVM to treat free surfaces, deformable boundaries, moving interfaces. Special techniques such as the volume of fluid (VOF) [31-33] and level set (LS) [34,35] are usually employed to track changing interfaces or free surfaces. For both CFD and CSD solvers, the treatment of pre-defined meshes introduces another classification of FSI analysis. It is generally a challenging task to generate mesh for situations with complex geometries or moving boundaries. Some additional complicated mathematical transformations are usually required, and this can be even more computationally expensive than solving the problem itself. Moreover, for implementing the interaction of fluid and structure in FSI, the precise location of the fluid-structure interface and information exchanges between the two parts also need to be taken into consideration.

The arbitrary Lagrangian-Eulerian (ALE) description of the finite element method is also widely used as a monolithic approach for dealing with FSI problems [36,37]. In ALE, the fluid sub-domain is discretized with a moving mesh that may fit the solid boundary. The equations for the fluid flow are solved at the arbitrarily moving nodes rather than at fixed points (as in the Eulerian grid-based methods like FDM and FVM), so that the fluid meshes actually follow the structural deformations. However, the large deformations of the fluid domain require the regeneration of fluid mesh that may increase the algorithmic complexity together with the computational cost. It is sometimes very difficult to re-mesh when a large structural deformation or displacement occurs in the simulation, especially in the presence of complicated interface geometry [38].

Some other grid-based or mesh reduced techniques have also been developed to deal with FSI problems. For example, some researchers applied the boundary element method (BEM) [39,40] to model liquid sloshing problems. However, the simulations of FSI problems using BEM are usually limited to relatively simple geometries and physics [41]. Vreman [42,43] applied the so-called overset grid method to treat FSI problems, i.e., particle-laden pipe flows. This method is based on two sets of background meshes including a fixed mesh for the fluid and a body-fitted mesh for each particle, and therefore the overset grid method for FSI is actually a partitioned approach. In Vreman's work, the velocity and pressure on different background grids are coupled by third-order Lagrange interpolations. As such, the frequent generation and deformation of computational grids due to moving boundaries can be avoided. However, the overset grid method is still under development, further improvements and validations are necessary.

1.3 SPH as a meshfree particle method

Recently, meshfree and particle methods have been demonstrated to have special advantages over the grid-based methods for modeling FSI problems with free surfaces, deformable boundaries and moving interfaces [5,44,45]. The key idea of the meshfree methods is to provide accurate and stable numerical solutions for integral equations or PDEs with all kinds of possible boundary conditions using a set of arbitrarily distributed nodes or particles. The history, development, theory and applications of the major existing meshfree methods have been addressed in some monographs and review articles [5,17,44-46]. Among these meshfree methods, the smoothed particle hydrodynamics (SPH) and moving particle semi-implicit (MPS) are two widely used particle methods for treating FSI problems. The SPH method was originally invented by Gingold and Monaghan [47] and Lucy [48] for modeling astrophysical problems in three-dimensional open space, and nowadays it has been widely used in engineering and sciences [5,49]. The MPS method was initially proposed by Koshizuka et al. [50,51] to simulate incompressible flows involving fluid-structure interactions. These two methods are truly Lagrangian, meshfree and particle methods and they can be categorized into two classes of weakly compressible and incompressible ones. The weakly compressible approach such as weakly compressible SPH (WCSPH) [5,49] solves an appropriate equation of state

by treating the fluid as weakly compressible. This approach is simple in concept, easy in computer implementation and capable of obtaining reasonable flow patterns, hence it is widely used for modeling FSI problems. The incompressible approach, such as MPS or incompressible SPH (ISPH) [52,53] solves a Poisson pressure equation (PPE) through application of the Chorin's projection method [54]. Therefore, these are also regarded as the projection-based particle methods. For more information about the MPS and SPH methods, one may refer to some excellent reviews [5,49,55-60].

As a truly meshfree and Lagrangian method, SPH has natural advantages for modeling FSI problems with large deformations and rapidly moving interfaces or free surfaces [61-68]. It is often regarded as the earliest modern meshfree particle method since no grid or mesh is used in SPH simulations and the collective movement of SPH particles is similar to the movement of a liquid or gas flow. SPH allows a straightforward handling of very large deformations and free surfaces since the connectivity between particles are generated as a part of the computation and can change with time. Due to these attractive features, SPH is very suitable for dealing with problems involving complicated nonlinear and often multiphase phenomena [11,64,69]. Without involving highly complicated algorithms in grid-based schemes, SPH can achieve results very close to the reference data (experimental or analytical solution) in validation cases. Therefore, for modeling violent FSI problems, SPH has been attracting more and more attentions compared to other grid-based methods. As mentioned in ref. [57], the recent developments in the numerical features of SPH has made it more credible and attractive to mathematicians whose previous interests are mainly focused on traditional and well-established approaches like FEM and FVM.

After the developments of several decades, the SPH has been proven to be a very effective alternate approach for modeling FSI problems. Here we briefly review some recent progresses of SPH regarding to the accuracy, efficiency, stability and coupling issues.

1.3.1 Accuracy of SPH

During the past decades, different techniques have been proposed to restore the particle consistency and hence to improve the SPH approximation accuracy. Some of them involve reconstruction of a new smoothing function so as to satisfy the discretized consistency conditions. One typical example is the reproduced kernel particle method (RKPM) proposed by Liu and his co-workers [44,45]. Recently, one popular way is to construct improved SPH approximation schemes based on Taylor series expansion on the SPH approximation of a function and/or its derivatives. Typical examples include the corrective smoothed particle method (CSPM) by Chen and Beraun [70] and the finite particle method (FPM) by Liu et al. [71,72]. Batra and Zhang [73,74] concurrently developed a similar idea to FPM, which is called the modified SPH (MSPH), to deal with the problems in solid mechanics. Fang et al. [75,76] further improved this idea and developed a regularized Lagrangian finite point method for simulating incompressible viscous flows. Asprone et al. [77,78] also started from the original formulation of the finite particle method and developed a so-called modified finite particle method (MFPM) for modeling elastostatics and elastodynamic problems. It is noted that both the CSPM and FPM need to solve matrix equations, which may further lead to numerical instability or unexpected termination of the simulation. To deal with this problem, Zhang et al. [79,80] developed a decoupled finite particle method (DFPM) that does not need to solve matrix equations but possessing better accuracy than the conventional SPH. Recently, Huang et al. [81,82] developed a kernel interpolation formulation that is called the kernel gradient free SPH (KGF-SPH), in which the kernel derivatives are never used and the kernel interpolations are flexible when choosing kernel functions.

1.3.2 Efficiency of SPH

For applications of SPH in some practical problems, the expensive computational costs have been hindering the further development of SPH. To save computational costs, different high-performance computing techniques have been applied in SPH simulations including MPI [83-85], OpenMP [86,87], OpenCL [88], CUDA [89-91], and so on. One other way to improve the efficiency of SPH simulations is to use the multiple spatial resolutions. The large number of particles and the distribution of particles with single spatial resolution result in prohibitive CPU times and memory requirements, and hence some researchers turn to the use of a variable spatial particle distribution [92,93]. Recently, a more general and challenging treatment is the dynamical refinement through the mechanism of particle splitting/coalescing [94-96], or named adaptive particle resolution [97-99]. Feldman and Bonet [100] first proposed a particle refinement technique in which coarse or parent particles are split into several smaller or children particles to locally increase the spatial resolution. In other regions, the coarse particles are used for simulation and hence a huge computational cost can be saved. This technique is further developed by López et al. [101] through enforcing conservation of the change rate of density and thus higher accuracy can be obtained. This dynamic refinement algorithm can be further improved by incorporating a coarsening technique. For example, Vacondio et al. [94-96] developed a coalescing technique, in which children particles are coalesced pairwise into parent particles by conserving linear momentum and mass. Barcarolo et al. [97] developed another coalescing technique by retaining parent particles in splitting regions

instead of removing them.

1.3.3 Modeling incompressible flows

One of the well-known drawbacks of WCSPH is the spurious pressure oscillations (sometimes also regarded as a kind of numerical instability), which may arise from many reasons including the one where a stiff equation of state is used, the SPH approximation itself are not very accurate [5], and so on. Recently, many improvements on SPH have been proposed to deal with this problem. The first one is to calculate the pressure implicitly from solving the pressure Poisson's equation (PPE, see more about PPE in refs. [50,102]), rather than from an artificial equation of state as in WCSPH. This leads to the so-called incompressible smoothed particle hydrodynamics (ISPH) method [52,53]. Unlike WCSPH, the particle density in ISPH remains unchanged, ensuring the rigorous incompressibility of the fluid. Different studies [53,103] have been reported on the comparison of ISPH with WCSPH, in which ISPH has shown a good performance in predicting the pressure and obtaining smooth velocity fields. Due to these advantages of ISPH, many researchers have also focused on developing the methodology of ISPH together with applications on modeling violent fluid-structure interactions [64,104-106]. Since the pressure is calculated as a function of density in WCSPH, another approach for dealing with the noisy pressure in SPH is to renormalize the density of particles after many time steps [17]. Antuono et al. [107,108] added a smoothing density term to the continuity equation (δ-SPH), which can help remit the density fluctuations in SPH. Next, a popular way to deal with the noisy pressure is to include the Riemann problem within SPH, i.e., including the shock-capturing techniques within SPH [109-111]. For example, Vila [109] proposed an SPH approximation technique in the ALE context and solved the PDEs based on a transport operator and flux vectors. Due to the advantages in capturing the shock waves and smoothing the pressure fields, the approximate Riemann solvers in SPH have been successfully applied to a variety of FSI problems including wave impact on structures, liquid sloshing, and objects impacting the fluid surface [93,112,113].

1.3.4 Modeling structural deformations

When applying SPH to model FSI problems, the deformation of structure should be properly treated. To describe the structural deformations in FSI, different approaches based on the SPH method have been proposed. One common way is to adopt a coupling strategy where the fluid is modeled using SPH while the solid is modeled using other meshfree or grid-based methods, and this will be discussed in the next subsection. Another popular way is to introduce the constitutive equation for the solid in the SPH contexts [114-116]. Some researchers have also developed various SPH models for describing the responses of different structures, such as the shell SPH for shell structures [117,118]. The treatment of structural deformations in FSI with SPH will be discussed detailedly in the following sections. As the explosion and impact problems are also important applications of SPH, we further introduced the SPH modeling of structural deformations in explosion and impact problems. Numerical simulation of this kind of problems is one of the formidable but attractive tasks in computational solid mechanics and computational fluid mechanics. The typical numerical examples range from Taylor bar impacting on a solid wall and spherical projectile/bumper collision/penetration [63,119] to contact explosion [120] and explosive forming [121], etc. Libersky and his co-workers [63,122] carried out the pioneering work of applying the SPH method to such high strain hydrodynamic problems. Later, Liu et al. [123-125] have extended the SPH method for simulating impact and explosion phenomena and developed the adaptive smoothed particle hydrodynamics method (ASPH) [126]. Recently, Zhang and Liu's group [68,121,127-129] proposed the modified SPH for high velocity impact problem and the density adaptive SPH for explosive forming problem. The explosion phenomenon in ocean engineering is a very important branch of FSI problems. It is worth noting that Zhang et al. [120,130-132] have developed different numerical models addressing the applications of SPH on the underwater explosion problems.

1.3.5 Coupling of SPH with other methods

Recently, the coupling approaches of SPH with other methods have been developed rapidly to save the computational cost and to achieve better accuracy and/or flexibility. There are many implementation methodologies for the coupling of SPH with other methods. The first one is to model the fluid flow in a local small area with SPH while in other larger areas with grid-based method or other particle-based methods. Marrone et al. [133,134] coupled SPH with FVM for modeling free surface flows, in which the FVM solver is applied to resolve the bulk flow and the wall regions, whereas the SPH solver is implemented in the free surface region to capture the details of the front evolution. The other more popular coupling methods are dedicated to the modeling of FSI problems. In these treatments, the fluid flow is usually modeled by SPH, and the structure is modeled by other methods such as FEM and DEM. Many researchers [135-138] have coupled SPH with FEM for modeling different FSI problems including the flow past a fixed cylinder with a flexible bar, the collapse of water column onto an elastic obstacle, a structure impacting the water reservoir, the flow in a sloshing tank interacting with an elastic body and so on. Some other researchers [139-141] have successfully coupled SPH with DEM for FSI problems where SPH is applied to model the fluid and the structural deformation or failure is simulated with DEM. Furthermore, SPH can also be coupled with some other methods to treat FSI problems.

For example, Yang et al. [142-144] proposed the coupling of SPH with element bending group (EBG) for modeling the interaction between viscous flows and flexible structures.

This article is organized as follows. In sect. 2, the basic concepts of SPH with conventional particle approximation and some higher order approximation schemes are introduced. The implementations of FSI in SPH are addressed in sect. 3. In sect. 4, the SPH coupled with FEM, FVM, EBG and with other methods for dealing with FSI are discussed in detail. In sect. 5, some important applications of SPH in FSI problems are demonstrated. These applications include FSI problems with rigid, elastic and flexible structures, FSI problems with granular materials and FSI problems with extremely intensive loadings. This paper concludes in sect. 6 together with remarks on SPH modeling of FSI problems.

2 SPH methodology

2.1 Basic concepts of SPH with conventional approximations

In SPH method, the governing partial differential equations are approximated in two steps, the kernel approximation and the particle approximation. In kernel approximation, the kernel (or smoothing) function W is introduced to describe the interaction between SPH particles. A field function $f(\mathbf{x})$ and its spatial derivative $\nabla \bullet f(\mathbf{x})$ at position $\mathbf{x}$ can then be written as:

$$\langle f(\mathrm{x})\rangle = \int_{\Omega} f(\mathbf{x}')W(\mathbf{x}-\mathbf{x}',h)\mathrm{d}\mathbf{x}', \tag{1}$$

$$\langle \nabla \cdot f(\mathbf{x})\rangle = -\int_{\Omega} f(\mathbf{x}')\nabla W(\mathbf{x}-\mathbf{x}',h)\mathrm{d}\mathbf{x}', \tag{2}$$

where $<\ >$ denotes the SPH approximation, and h is the smoothing length defining the support domain of the kernel function W. Ω represents the problem space whose radius is taken as several times of h according to different smoothing functions. The kernel function W should be chosen as an even function and should also satisfy many conditions including the normalization condition, Delta function property and compact condition that are shown by eqs. (3)-(5) respectively,

$$\int_{\Omega} W(\mathbf{x}-\mathbf{x}',h)\mathrm{d}\mathbf{x}' = 1, \tag{3}$$

$$\lim_{h\to 0} W(\mathbf{x}-\mathbf{x}',h) = \begin{cases} \infty, \mathbf{x} = \mathbf{x}', \\ 0, \mathbf{x} \neq \mathbf{x}', \end{cases} \tag{4}$$

$$W(\mathbf{x}-\mathbf{x}',h) = 0, \text{ when } |\mathbf{x}-\mathbf{x}'| > \kappa h, \tag{5}$$

where κ is a constant and κh is used to define the effective area of the smoothing function (the radius of the problem space). The selection of the kernel function has a significant influence on the computational accuracy. In SPH kernel approximation, there are two widely used smoothing functions including the cubic spline function [145] and the Gaussian function [47]. The cubic spline function is given by

$$W(R,h) = \alpha_{\mathrm{d}} \times \begin{cases} \frac{2}{3} - R^2 + \frac{1}{2}R^3, & 0 \le R < 1, \\ \frac{1}{6}(2-R)^3, & 1 \le R < 2, \\ 0, & R \ge 2, \end{cases} \tag{6}$$

where α_{d} is a dimension-dependent constant, and it is $1/h$ or $15/7\pi h^2$ in one or two-dimensional space for cubic spline function. R is the distance between two particles normalized by the smoothing length. The Gaussian function is given by

$$W(S,h) = \alpha_{\mathrm{d}} \mathrm{e}^{-S^2}, \tag{7}$$

where $S = |\mathbf{x}-\mathbf{x}'|/h$ and α_{d} is $1/\pi^{1/2}h$ or $1/\pi h^2$ in one or two-dimensional space for Gaussian function. Recently, different kernel functions in SPH have been proposed to achieve better accuracy and stability, and one may see more kernel functions in refs. [5, 56].

According to the kernel properties of

$$\int_{\Omega} f(\mathbf{x}) \cdot \nabla W(\mathbf{x}-\mathbf{x}',h)\mathrm{d}\mathbf{x}' = 0,$$

the symmetric and anti-symmetric forms of the kernel approximation can be obtained as:

$$\langle \nabla \cdot f(\mathbf{x})\rangle = \int_{\Omega} [f(\mathbf{x}') - f(\mathbf{x})] \cdot \nabla W(\mathbf{x}-\mathbf{x}',h)\mathrm{d}\mathbf{x}', \tag{8}$$

$$(\nabla \cdot f(\mathbf{x})) = \int_{\Omega} [f(\mathbf{x}') + f(\mathbf{x})] \cdot \nabla W(\mathbf{x}-\mathbf{x}',h)\mathrm{d}\mathbf{x}'. \tag{9}$$

In practical applications, eq. (8) is more often used for the discretization of the continuum equation. It is well known that the kernel function can be truncated by the boundary of the computational domain, and this kernel truncation by the boundary has significant influence on the accuracy of the kernel approximation. Eq. (8) can somewhat reduce the errors of boundary truncations, as shown in ref. [146].

The particle approximation step of SPH involves representing the problem domain with a set of particles and then estimating field variables on this set of particles. The illustration of a two-dimensional problem domain Ω represented by a set of particles can be seen in Figure 1. These particles are associated with the field properties, and can be used not only for integration, interpolation or differencing, but also for representing the material. Each particle is given a fixed lumped volume V_i while it does not have a fixed shape. These particles can be either fixed in an Eulerian frame or move in a Lagrangian frame.

By summing up the over-all neighboring particles around particle i within its support domain, the kernel approximations of a field function and its spatial derivative can be given in a discretized form as:

$$\langle f(\mathbf{x}_i)\rangle = \sum_{j=1}^{N} \frac{m_j}{\rho_j} f(\mathbf{x}_j)W(\mathbf{x}_j-\mathbf{x}_i), \tag{10}$$

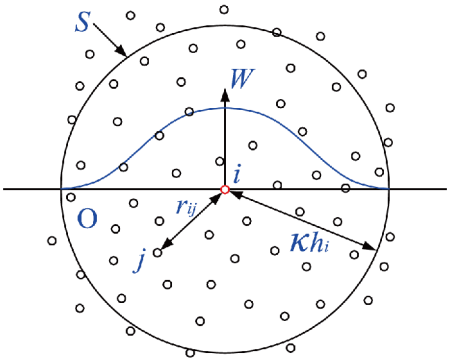

Figure 1 (Color online) Illustration of particle distribution around particle i in two-dimensional space. κh_i represents the radius of the support domain S of the interested particle i.

$$\langle \nabla \cdot f(\mathbf{x}_i) \rangle = \sum_{j=1}^{N} \frac{m_j}{\rho_j} f(\mathbf{x}_j) \nabla_i W_{ij}, \tag{11}$$

where m_j and ρ_j are the mass and density of a particle j, N is the total number of the neighboring particles for a certain particle i. In the following sections, the SPH approximation sign < > is ignored for the sake of conciseness.

The particle approximation of the integral is a very important technique in SPH that gives SPH natural advantages in capturing the large motion of the materials since no background mesh is used for the integration. The introduction of particle mass and density into the governing equations can be conveniently applied to hydrodynamic problems where the density ($\rho_i = m_i / V_i$) is a key field variable. This makes the SPH method rather attractive for dynamic fluid flow problems. However, the particle approximation technique may also introduce the accuracy loss and instability problems. If the particles distribute non-uniformly in the support domain of the interested particle i, there may not be enough particles for approximating the field variables of the particle i and this brings the particle inconsistency problem. As for the instability introduced by the particle approximation, an important reason is that the discrete summation is only taken over the particles themselves. In meshfree methods, the number of sampling points for the integration should be more than the field nodes (particles), especially for meshfree methods based on weak forms for solid mechanics problems [5]. Otherwise, some kinds of instability problems may occur in this situation.

2.2 High order approximation schemes

It is noted that the conventional SPH method is associated with low accuracy, and the particle approximation scheme expressed in eqs. (10) and (11) are not able to reproduce a linear function or even a constant [71]. Thus, the reduced accuracy of conventional SPH has been hindering its further developments in applications requiring high accuracy. Different approaches have been proposed to improve the SPH approximation accuracy. Here we discussed several typical methods including the finite particle method (FPM) by Liu et al. [71,72], the corrective smoothed particle method (CSPM) by Chen and Beraun [70], the kernel gradient free SPH (KGF-SPH) by Huang et al. [81,82] and the decoupled finite particle method (DFPM) by Zhang et al. [79,80].

2.2.1 *Finite particle method*

The finite particle method (FPM) developed by Liu and his co-workers is an improved and general form of the conventional SPH. The derivation of FPM can be summarized as follows. Performing Taylor series expansion at a nearby point $\mathbf{x}_i$ and retaining the first order derivatives, a sufficiently smooth function $f(\mathbf{x})$ at point $\mathbf{x}$ can be expressed as:

$$f(\mathbf{x}) = f_i + f_{i,\alpha}(\mathbf{x}^\alpha - \mathbf{x}_i^\alpha) + r((\mathbf{x} - \mathbf{x}_i)^2), \tag{12}$$

where f_i and $f_{i,\alpha}$ are defined as $f_i = f(\mathbf{x}_i)$, and $f_{i,\alpha} = (\partial f / \partial \mathbf{x}^\alpha)_i$. Multiplying both sides of eq. (12) with a kernel $W(\mathbf{x} - \mathbf{x}_i)$ and $\nabla W(\mathbf{x} - \mathbf{x}_i)$, and integrating over the problem space, the following equations can be obtained,

$$\int_\Omega f(x) W(\mathbf{x} - \mathbf{x}_i) \mathrm{d}\mathbf{x} = f_i \int_\Omega W(\mathbf{x} - \mathbf{x}_i) \mathrm{d}\mathbf{x} + \nabla f_i \int_\Omega (\mathbf{x} - \mathbf{x}_i) W(\mathbf{x} - \mathbf{x}_i) \mathrm{d}\mathbf{x}, \tag{13}$$

$$\int_\Omega f(\mathbf{x}) \nabla W(\mathbf{x} - \mathbf{x}_i) \mathrm{d}\mathbf{x} = f_i \int_\Omega \nabla W(\mathbf{x} - \mathbf{x}_i) \mathrm{d}\mathbf{x} + \nabla f_i \int_\Omega (\mathbf{x} - \mathbf{x}_i) \nabla W(\mathbf{x} - \mathbf{x}_i) \mathrm{d}\mathbf{x}, \tag{14}$$

where Ω denotes the problem space and will be ignored for the sake of conciseness in the following equations. According to eqs. (13) and (14), the following matrix equation applies

$$\begin{Bmatrix} f_i \\ \nabla f_i \end{Bmatrix} = \mathbf{L}^{-1} \begin{bmatrix} \int f(\mathbf{x}) W(\mathbf{x} - \mathbf{x}_i) \, \mathrm{d}\mathbf{x} \\ \int f(\mathbf{x}) \nabla W(\mathbf{x} - \mathbf{x}_i) \, \mathrm{d}\mathbf{x} \end{bmatrix}, \tag{15}$$

$$\mathbf{L} = \begin{bmatrix} \int W(\mathbf{x} - \mathbf{x}_i) \, \mathrm{d}\mathbf{x} & \int (\mathbf{x} - \mathbf{x}_i) W(\mathbf{x} - \mathbf{x}_i) \, \mathrm{d}\mathbf{x} \\ \int \nabla W(\mathbf{x} - \mathbf{x}_i) \, \mathrm{d}\mathbf{x} & \int (\mathbf{x} - \mathbf{x}_i) \nabla W(\mathbf{x} - \mathbf{x}_i) \, \mathrm{d}\mathbf{x} \end{bmatrix}. \tag{16}$$

It is important to highlight that if $\mathbf{L}$ is replaced with a unit matrix, eq. (15) exactly represents the conventional SPH approximations for f and its derivatives. With the corrective matrix $\mathbf{L}$, the conventional SPH method can be improved to have second order accuracy as the first derivatives are retained in eq. (12).

2.2.2 *Corrective SPH and kernel gradient correction*

Based on the Taylor series expansion on the SPH approximations, Chen and Beraun [70] developed the corrective

smoothed particle method (CSPM) to construct improved SPH approximation schemes and further applied it for nonlinearly dynamic problems. By only correcting the derivative of the kernel functions, the kernel gradient correction technique (KGC) [11,121,147] is widely applied in SPH simulations. Although CSPM and KGC technique is proposed earlier than FPM or other modified versions of SPH, such approximation schemes can be regarded as the reduced forms of FPM. For example, in eq. (14), moving the first term on the right-hand-side (RHS) to the left-hand-side (LHS), the CSPM approximations for the derivatives of f in three-dimensional space are given by

$$\begin{pmatrix} f_{i,x} \\ f_{i,y} \\ f_{i,z} \end{pmatrix} = \mathbf{M}^{-1} \begin{pmatrix} \int (f(\mathbf{x}) - f_i) W_x' \mathrm{d}\mathbf{x} \\ \int (f(\mathbf{x}) - f_i) W_y' \mathrm{d}\mathbf{x} \\ \int (f(\mathbf{x}) - f_i) W_z' \mathrm{d}\mathbf{x} \end{pmatrix}, \tag{17}$$

$$\mathbf{M} = \begin{pmatrix} \int (x - x_i) W_x' \mathrm{d}V & \int (y - y_i) W_x' \mathrm{d}V & \int (z - z_i) W_x' \mathrm{d}V \\ \int (x - x_i) W_y' \mathrm{d}V & \int (y - y_i) W_y' \mathrm{d}V & \int (z - z_i) W_y' \mathrm{d}V \\ \int (x - x_i) W_z' \mathrm{d}V & \int (y - y_i) W_z' \mathrm{d}V & \int (z - z_i) W_z' \mathrm{d}V \end{pmatrix}. \tag{18}$$

If neglecting the first term on the RHS of eq. (14) (this is true for interior area of the computational domain, see ref. [71] for more details), the KGC approximations for the derivatives of f in three-dimensional space are given by

$$\begin{pmatrix} f_{i,x} \\ f_{i,y} \\ f_{i,z} \end{pmatrix} = \mathbf{M}^{-1} \begin{pmatrix} \int f(\mathbf{x}) W_x' \mathrm{d}\mathbf{x} \\ \int f(\mathbf{x}) W_y' \mathrm{d}\mathbf{x} \\ \int f(\mathbf{x}) W_z' \mathrm{d}\mathbf{x} \end{pmatrix}. \tag{19}$$

Here we only give the CSPM and KGC approximations derived from the FPM formulations, and one may see more details about these two techniques in refs. [70,127]. From the derivation of CSPM and the relevant mathematical tests in ref. [71], it is seen that in a one-dimensional space, CSPM has the same accuracy with SPH for approximating the interior particles of a computational domain. For the boundary regions, CSPM restores the C_0 kernel consistency (1st order accuracy) by retaining the non-unity denominator. That is to say for dealing with the boundary regions or non-uniform particle distributions, CSPM can obtain higher accuracy than SPH while it could not restore C_1 kernel consistency or say achieve second order accuracy as FPM.

2.2.3 *Kernel gradient free SPH*

Huang et al. [81,82] developed a kernel gradient free (KGF) SPH method in which the kernel gradient is not necessary in the whole simulation. The following gives the typical approximation formulae in KGF-SPH. Multiplying both sides of eq. (12) with the $(\mathbf{x} - \mathbf{x}_i) \cdot W(\mathbf{x} - \mathbf{x}_i)$ and integrating over the problem space, we can have

$$\begin{aligned} &\int_\Omega f(\mathbf{x})(\mathbf{x} - \mathbf{x}_i) W(\mathbf{x} - \mathbf{x}_i) \mathrm{d}\mathbf{x} \\ &= f_i \int_\Omega (\mathbf{x} - \mathbf{x}_i) W(\mathbf{x} - \mathbf{x}_i) \mathrm{d}\mathbf{x} \\ &\quad + \nabla f_i \int_\Omega (\mathbf{x} - \mathbf{x}_i)^2 W(\mathbf{x} - \mathbf{x}_i) \mathrm{d}\mathbf{x}. \end{aligned} \tag{20}$$

For the sake of conciseness, the kernel function $W(\mathbf{x} - \mathbf{x}_i)$ is denoted as W in the following equations. By solving eqs. (13) and (20) simultaneously, the matrix equation in three-dimensional space can be given by

$$\begin{Bmatrix} f_i \\ \nabla f_i \end{Bmatrix} = K^{-1} \begin{bmatrix} \int f(\mathbf{x}) W \mathrm{d}\mathbf{x} \\ \int f(\mathbf{x})(\mathbf{x} - \mathbf{x}_i) W \mathrm{d}\mathbf{x} \end{bmatrix}, \tag{21}$$

$$K = \begin{bmatrix} \int W \mathrm{d}V & \int (x - x_i) W \mathrm{d}V & \int (y - y_i) W \mathrm{d}V & \int (z - z_i) W \mathrm{d}V \\ \int (x - x_i) W \mathrm{d}V & \int (x - x_i)(x - x_i) W \mathrm{d}V & \int (x - x_i)(y - y_i) W \mathrm{d}V & \int (x - x_i)(z - z_i) W \mathrm{d}V \\ \int (y - y_i) W \mathrm{d}V & \int (y - y_i)(x - x_i) W \mathrm{d}V & \int (y - y_i)(y - y_i) W \mathrm{d}V & \int (y - y_i)(z - z_i) W \mathrm{d}V \\ \int (z - z_i) W \mathrm{d}V & \int (z - z_i)(x - x_i) W \mathrm{d}V & \int (z - z_i)(y - y_i) W \mathrm{d}V & \int (z - z_i)(z - z_i) W \mathrm{d}V \end{bmatrix}. \tag{22}$$

Based on eqs. (21) and (22), the field function and it derivatives can be attained without calculating the gradient of the kernel function. This greatly widens the selection of the kernel function. The corrective matrix in KGF-SPH approximation is invertible and hence KGF-SPH can effectively avoid the ill-conditioned matrices likely to occur in FPM and CSPM simulations. Hence, the KGF-SPH simulations can be more stable than other modified SPH with matrix inversion. Besides, the corrective matrix in KGF-SPH has a good symmetry, which can simplify the solution process of the matrix equation.

2.2.4 *Decoupled finite particle method*

The decoupled finite particle method proposed by Zhang et al. [79,80] can be regarded as simplified form of FPM. It is noted that the approximations of f and its derivatives are coupled together in CSPM, KGC and FPM. These couplings are implemented through the corrective matrix $\mathbf{L}$ or $\mathbf{M}$. If the

computational domain is represented with a finite number of particles, the resultant FPM, CSPM and KGC particle approximations are not sensitive to irregular particle distribution. This is a huge improvement to the conventional SPH method that suffers from problems like boundary deficiency and particle-distribution sensitivity. However, the corrective matrices in FPM, CSPM and KGC can be ill-conditioned when modeling some practical problems with singularly distributed particles (extremely disordered particles). This leads to a numerical instability, and may even cause the breakdown of the simulation.

In FPM, CSPM and KGC, when estimating a derivative in a certain direction, it is reasonable to assume that the contribution from the self-direction is dominant and the contributions from the other directions are negligible. This is similar to an estimation of the partial derivatives in the finite difference method, in which the partial derivatives in a certain direction is frequently replaced with the finite differencing along the same direction [148]. Based on these considerations, after neglecting the contributions from the other directions, the corrective matrix **L** in FPM in three-dimensional space can be

$$\mathbf{L}'=\begin{pmatrix} \int W\mathrm{d}V & 0 & 0 & 0 \\ 0 & \int (x-x_i)W_x'\mathrm{d}V & 0 & 0 \\ 0 & 0 & \int (y-y_i)W_y'\mathrm{d}V & 0 \\ 0 & 0 & 0 & \int (z-z_i)W_z'\mathrm{d}V \end{pmatrix}^{-1}. \tag{23}$$

This new corrective matrix $\mathbf{L}'$ is diagonally dominant and decouples the approximations of the field function f and its derivatives. For some specific applications, if only the derivatives of a field function need to be approximated, the first element of the matrix $\mathbf{L}'$ is not necessary in the numerical simulations. We put all these elements here to show that the approximations of a field function and its derivatives in the presented method are completely independent. Therefore, a correction with $\mathbf{L}'$ leads a decoupled finite particle method (DFPM), in which the particle approximations of the field function f and its derivatives can be written as:

$$\begin{cases} f_i=\dfrac{\sum\limits_{j=1}^{N} f_j W_{ij}\Delta V_j}{\sum\limits_{j=1}^{N} W_{ij}\Delta V_j}, \quad f_{i,x}=\dfrac{\sum\limits_{j=1}^{N} f_j \dfrac{\partial W_{ij}}{\partial x_i}\Delta V_j}{\sum\limits_{j=1}^{N} x_{ji}\dfrac{\partial W_{ij}}{\partial x_i}\Delta V_j}, \\ f_{i,y}=\dfrac{\sum\limits_{j=1}^{N} f_j \dfrac{\partial W_{ij}}{\partial y_i}\Delta V_j}{\sum\limits_{j=1}^{N} y_{ji}\dfrac{\partial W_{ij}}{\partial y_i}\Delta V_j}, \quad f_{i,z}=\dfrac{\sum\limits_{j=1}^{N} f_j \dfrac{\partial W_{ij}}{\partial z_i}\Delta V_j}{\sum\limits_{j=1}^{N} z_{ji}\dfrac{\partial W_{ij}}{\partial z_i}\Delta V_j}. \end{cases} \tag{24}$$

The asymmetric form of eq. (24) is often used in practical problems, which applies

$$\begin{aligned} f_{i,x}&=\frac{\sum\limits_{j=1}^{N}(f_j-f_i)\dfrac{\partial W_{ij}}{\partial x_i}\Delta V_j}{\sum\limits_{j=1}^{N} x_{ji}\dfrac{\partial W_{ij}}{\partial x_i}\Delta V_j}, \\ f_{i,y}&=\frac{\sum\limits_{j=1}^{N}(f_j-f_i)\dfrac{\partial W_{ij}}{\partial y_i}\Delta V_j}{\sum\limits_{j=1}^{N} y_{ji}\dfrac{\partial W_{ij}}{\partial y_i}\Delta V_j}, \\ f_{i,z}&=\frac{\sum\limits_{j=1}^{N}(f_j-f_i)\dfrac{\partial W_{ij}}{\partial z_i}\Delta V_j}{\sum\limits_{j=1}^{N} z_{ji}\dfrac{\partial W_{ij}}{\partial z_i}\Delta V_j}. \end{aligned} \tag{25}$$

It is clear that the DFPM involves normalization on the approximation of the field function f and its derivatives with the smoothing function and its derivatives respectively. As only simple normalizations are used, DFPM inherits advantages from the conventional SPH and is flexible, cost-effective and easy in coding. Also as DFPM possesses major features of FPM, it is more accurate than the conventional SPH and is not sensitive to particle distribution or selection of the smoothing function and smoothing length. More importantly, no matrix inversion is required in DFPM, which is different from FPM, CSPM and KGC. Therefore, the ill-conditioned corrective matrices can be effectively avoided and this is very attractive for modeling practical problems, such as particulate flows.

3 Implementation of FSI in SPH

The key challenge in modeling FSI problems is the algorithm to implement the fluid-structure interaction, i.e., to exchange information between fluids and structures in a consistent and physical manner. As mentioned previously, most existing FSI algorithms are based on the partitioned approach, and the equations governing the fluid flow and the movement of the structure are solved separately with a CFD solver for fluids and a CSD solver for structures. The material interface is thus the boundary of the fluid area and the structure region. Moreover, the displacement, velocity, and stress need to be consistent across the material interface. One typical example is the coupled Eulerian-Lagrangian (CEL) [149], which involves both the Eulerian methods (e.g., FVM) and Lagrangian methods (e.g., FEM) in separate (or with some overlap) regions of the problem domain. One of the most common practices is to discretize solids in a Lagrangian frame, and fluids (or materials behaving like fluids) in an Eulerian frame. The Lagrangian region and Eulerian regions continuously interact with each other through a coupling

module in which the computational information is exchanged either by mapping or by special interface treatments between these two sets of grid. This partitioned approach leverages the advantages of CFD solver in modeling fluid flow and CSD solver in modeling structure deformation, and thus it is a straightforward and popular strategy in modeling FSI. As the interaction of fluid and structure is usually not implemented at each time step in a single solver, the partitioned approach is actually a weak coupling with delayed interaction. Moreover, in order to precisely locate the fluid-structure interface, an accurate and robust interface detection algorithm is necessary.

In SPH modeling of FSI problems, the SPH method can be used both in the fluid area and the structure area. This actually is a monolithic approach and the equations governing the fluid flow and the movement of the structure are solved simultaneously with a single SPH solver. The SPH method can also be coupled with other grid-based or particle-based methods. The fluid-structure interaction in this situation is thus a partitioned approach in which SPH is applied in the fluid area while the other method is used in the structure region or the other fluid region. The coupling of SPH with other methods as a partitioned FSI approach will be further addressed in the next section.

In this section, we focus on the pure SPH modeling of FSI problems as a monolithic approach. The material interface in FSI problems is actually a moving or deformable solid boundary. Hence, similar to the treatment of fixed solid walls in SPH, when treating material interface in FSI, ghost or virtual particles are commonly utilized to represent the material interface or interface region. Being different from the fixed solid boundary treatment in which non-slip or slippery boundary conditions need to be satisfied, the material interface treatment in FSI need to take the interface condition (consistency of displacement, velocity and stress) into consideration.

3.1 Treatment of fixed wall as a solid boundary

The fluid-rigid structure interaction is one of the most common FSI problems, in which the interface between a fixed wall and a fluid can be treated as a solid boundary. In this condition, the interaction between solid and fluid can be implemented directly according to different solid boundary treatment algorithms. Since the invention of SPH, the treatment of the fixed wall boundary has been a numerical focus, which keeps influencing the accuracy of SPH and hindering its further development in engineering and sciences.

The treatment of solid wall boundary in particle methods, such as molecular dynamics (MD) [150,151], dissipative particle dynamics (DPD) [152,153] and SPH, is very different from that of the grid-based methods. In some grid-based methods like FEM and FDM, the implementations of the solid boundary condition (e.g., Neumann boundary, Dirichlet boundary and mixed boundary) are usually straightforward [5]. It is common for MD and DPD to represent the solid boundary areas with fixed particles that can prevent the penetration of mobile particles into the solid boundaries and can also interact with the mobile particles with appropriate interaction models. In this way, some complex solid matrix and fluid-solid interface physics can be precisely modeled. Actually, the boundary techniques in MD and DPD can also be used in SPH to exert the slip or non-slip boundary conditions. However, the solid boundary treatment in SPH is more difficult as SPH is a continuum scale particle method where the field variables on boundaries, such as the pressure need to be directly calculated. There have been many proposals for solid boundary treatments in SPH and these approaches can be generally classified into three approaches: fictitious particle method, repulsive particle method and boundary integral method.

3.1.1 Representation of solid boundary area with fictitious particles

Fictitious (or virtual) particles are usually generated in the solid boundary areas to complete the missing support of the kernel. By this way, the boundary deficiency can be somewhat alleviated and higher simulation accuracy near the boundaries can be achieved. The mirror particle and dummy particle are two widely used fictitious particles. In mirror particle approach, a mirror image of the fluid particle is generated inside the boundary areas, as shown in Figure 2. The fluid particle near the boundary may interact with the mirror particle of itself and therefore the penetration of fluid particles into boundaries can be avoided since a particle cannot penetrate its mirror image. This approach is suitable for the boundaries with relatively simpler geometries, whereas it may meet some difficulties for applications on complex boundaries with sharp corners [57].

In general, the dummy particle approach is the most accepted one in handling a solid boundary. The dummy particles are generated at the beginning of the simulation and kept fixed in the boundary area or move with the boundary during the simulation process. The number of dummy particles should be properly chosen according to the support of the kernel function (usually three or more layers). The dummy particles inside the boundary can be associated with the boundary particles whose variables are calculated according to the governing equations, or associated with the projecting (intercalated) points that are intercalated from the interior fluid particles, as shown in Figure 3. For example, the pressure of the dummy particle can be obtained by

$$p_{\text{dummy}} = p_{\text{as}} + \rho\left[\frac{\mathrm{d}\mathbf{v}_{\text{b}}}{\mathrm{d}t}\cdot\mathbf{n}_{\text{b}} - \mathbf{g}\cdot\mathbf{n}_{\text{b}}\right]\varepsilon\Delta, \tag{26}$$

where the subscript as represents the associated particle

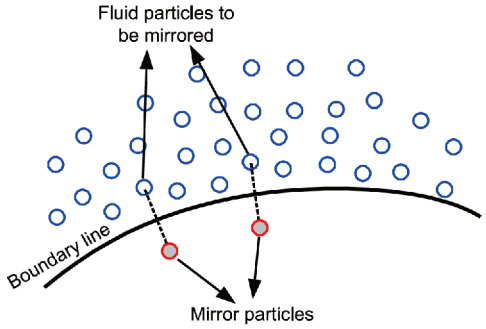

Figure 2 (Color online) Diagram of the mirror particle approach.

(boundary or projecting points), and b denotes the boundary particle. **n** denotes the unit normal vector of the boundary particle. $\varepsilon\Delta$ represents the distance between the inside dummy particle and the associated particle.

Despite the wide use of dummy particle method, it still carries some drawbacks. One important issue is that it is difficult for the dummy particles to prevent the penetration of real fluid particles into boundaries, and it may also create non-physical separation and boundary layers. Besides, to maintain the consistency of particle spacing, the spacing of dummy particles should be arranged close to that of the real particles. Hence, it may suffer from some difficulties when arranging the dummy particles inside slender bodies [136,154,155]. Fortunately, the multiple resolutions can be an efficient approach to deal with this problem by keeping consistent particle distribution around the boundary regions [156]. Recently, some efficient approaches on interpolating the field variables of fluids to the boundary based on the dummy particle method have been developed. Macia et al. [157] theoretically analyzed the enforcement of no-slip boundary condition in SPH methods and derived a consistent formulation. This new approach allows the implementation of no-slip boundary conditions consistently in many practical applications such as the viscous flows and diffusion problems. Based on a local force balance between wall and fluid particles, Adami et al. [158] developed a pressure boundary condition on the solid dummy particles to prevent the penetration of fluid particles.

3.1.2 Prevention of unphysical particle penetration with repulsive force models

The use of a repulsive force is an efficient approach to prevent the penetration of fluid particles into the boundary areas. In this model, the repulsive particles are located on the boundary exerting repulsive forces on the approaching particles. Monaghan [61] first used such particles with the repulsive force based on the Lennard-Jones (L-J) molecular potential, which is given by

$$\mathbf{F}_{ij}=\begin{cases}\alpha\left[\left(\dfrac{r_0}{r_{ij}}\right)^{\beta_1}-\left(\dfrac{r_0}{r_{ij}}\right)^{\beta_2}\right]\dfrac{\mathbf{r}_{ij}}{r_{ij}^2}, & \left(\dfrac{r_0}{r_{ij}}\right)\le 1,\\ 0, & \left(\dfrac{r_0}{r_{ij}}\right)>1,\end{cases} \tag{27}$$

where $\mathbf{F}ij$ is the repulsive force, and $\boldsymbol{r}ij$ denotes the position vector between a solid particle and an approaching fluid particle. α is set with the scale of the square of the largest fluid velocity, and r_0 is taken as the initial particle spacing. Parameters β_1 and β_2 are usually set as 12 and 4, respectively. The original L-J force experiences some drawbacks such as it is a highly repulsive force exerting infinite value on the particles approaching very close to each other. Also, it cannot apply a steady force on the particles moving parallel to the boundary. To consider the repulsive force acting on the particle moving parallel to the boundary, Monaghan and Kajtar [159] proposed a Laplace summation to calculate the repulsive force, and it can be given by

$$\begin{cases}f_x=\dfrac{1}{\Delta}\displaystyle\int_{-\infty}^{\infty}\frac{(x_a-q)\phi(r')}{r'}\mathrm{d}q,\\ f_y=\dfrac{y_a}{\Delta}\displaystyle\int_{-\infty}^{\infty}\frac{\phi(r')}{r'}\mathrm{d}q',\end{cases} \tag{28}$$

where $r'=\sqrt{(x_a-q)^2+y_a^2}$, $q'=x_a-q$. f_x and f_y represent the x and y components of the repulsive force acting on a fluid particle a. x_a and y_a denote the horizontal and perpendicular distances of the fluid particle to the boundary line. The repulsive force along the radial direction is given a magnitude of the function $\phi(r')$. The boundary particles are assumed to be equispaced with spacing Δ. This formula is used when the

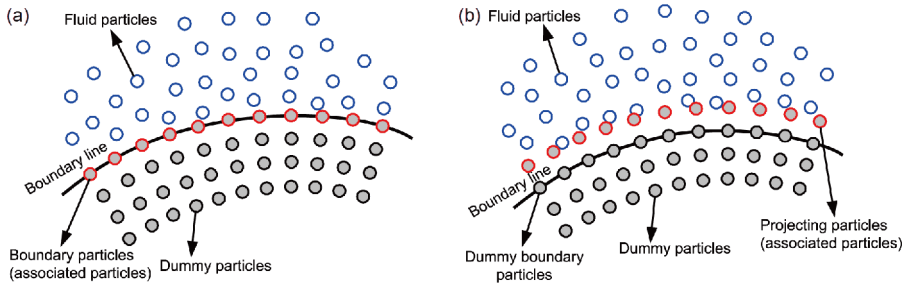

Figure 3 (Color online) Diagram of the dummy particle approach. The dummy particles can be associated with boundary particles (a) or projecting points (b).

boundary line is straight, and the integral is over the boundary line.

The aforementioned repulsive forces proposed by Monaghan et al. are based on the distance between the fluid particles to the boundary. Recently, Rogers and Dalrymple [160] proposed another alternate form of the repulsive boundary force considering the effects of the particle velocity. This repulsive force is given by

$$\mathbf{f} = \mathbf{n}R(\psi)P(\xi)\varepsilon(z, u_{\perp}), \tag{29}$$

where $\mathbf{n}$ is the unit vector normal to the solid boundary, $R(\Psi)$ is a repulsive function defined by the distance between a particle and the solid wall. The function $P(\xi)$ is used to exert a constant repulsive force on the particle traveling parallel to the wall. $\varepsilon(z, u_{\perp})$ is applied to adjust the magnitude of the force according to the local water depth z and the velocity of the water particle normal to the boundary $u_{\perp}$.

3.1.3 Boundary integral method for complex boundary conditions

For treating complex solid boundary conditions, the boundary integral method can be an effective approach. In this approach, the virtual particles are not used to represent the solid boundaries or to treat the kernel truncation problem. Instead, a wall renormalization factor in the SPH discrete interpolation is used to deal with the solid boundaries. Kulasegaram et al. [161] first proposed an approximate method to calculate the renormalization factor in order to implement such boundary integral method. Feldman and Bonet [100] further proposed an analytical method for treating simple wall shapes. Actually, in the boundary integral methods described earlier, the renormalization factor in the discrete SPH interpolation formula acts to exert a boundary force in the Navier-Stokes equations. Ferrand et al. [162] proposed a formulation of the differential operators to calculate the renormalization factor in a different way. In this method, the boundary condition can be implemented in a natural way through the boundary term of the new Laplacian operator. Amicarelli et al. [163] further developed this boundary integral model and successfully applied it for modeling violent 3D FSI problems. Recently, Leroy et al. [164] presented a semi-analytical wall boundary integral model based on the ISPH method, in which a non-homogeneous Neumann boundary condition on the pressure field is exactly implemented to solve the pressure Poisson equation such that an impermeability condition is applied on solid walls. The boundary integral approach or named the unified semi-analytical wall boundary condition has been developed rapidly these years for FSI problems. Owning to the short period of this method, more validation tests and more accurate and efficient approaches based on this method should be developed.

3.2 Treatment of FSI interface as a moving boundary

For modeling FSI problems with moving or deformable boundaries, an effective algorithm is required for efficiently describing the fluid-structure interface dynamics. It is somewhat different from the grid-based numerical methods in correctly detecting contact and effectively treating it in particle methods like SPH. The SPH particles can move freely and interact with different particles at each time step, and the particle aggregation and separation often occur in the moving interface regions. This further increases the difficulty in treating FSI interface by SPH.

3.2.1 Treatment of moving interface

When the structure moves or deforms under the interaction between fluid and structure, the FSI interface can be treated as a moving boundary. As such, the structure is discretized with virtual or real particles where particles from one material (fluid or solid) can influence, and also be influenced by the particles from the other material (solid or fluid), according to the SPH approximations. The aforementioned fictitious and repulsive particles can also be used to exert the interfacial conditions, i.e., boundary condition for one material. Figure 4 shows an example of the FSI interface at the initial stage, and at a later stage in the evolution. Initially the SPH particles are distributed regularly, and there is no intersection and deformation of particles. With the SPH evolution, fluid particles influence the structure particles in calculating the strain and strain rate, and vice versa the field

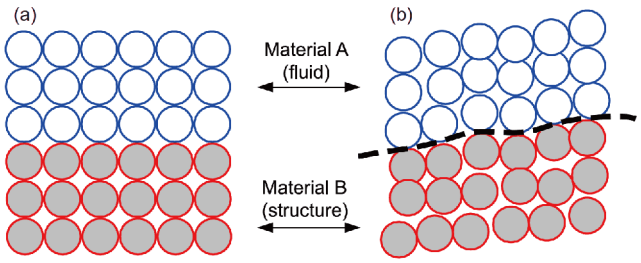

Figure 4 (Color online) Illustration of moving FSI interface in SPH particle model. (a) Initial SPH particle distribution, and (b) SPH particle distribution after evolution. Interaction between particles from different materials can introduce shear and tensile stress and can prohibit sliding and separation of different materials.

variables of fluid particles can be influenced by the moving structure. This interaction between the particles from different materials maintains the consistency of displacement, velocity and stress of interfacial particles, and can introduce shear and tensile stress that prevent sliding and separation of different materials. Special algorithms are required if an SPH model is used for the simulation of problems with sliding and separation.

A contact model is usually important in treating FSI interface as a moving boundary, which involves steps: 1) identifying the boundary, 2) detecting the contact and 3) applying repulsive contact forces. A convenient way to detect the particle-particle contact in FSI interface is to check the proximity of two approaching fluid and solid particles, and make a comparison with the summation of the smoothing lengths of the particles. As shown in Figure 5, the contact and penetration between two particles can be identified by

$$pe = \frac{kh_i + kh_j}{r_{ij}} \geq 1, \tag{30}$$

where r_{ij} is the distance between the particle i and the particle j. After detection of the contact and penetration, a restoring contact force needs to be applied along the centerline of the two particles (the position vector of particle i and particle j). There are different choices for restoring contact force, which is usually a function of penetration. One possible choice is the penalty force in Lennard-Jones form, as mentioned in sect. 3.1.

3.2.2 *Restoring interface consistency*

In treating the FSI interface as a moving boundary, the discontinuity at the interface or called large density ratio is an important issue. The pressure instability is very common in the moving interface regions, which is caused by the free movement of the particles. Different from the grid-based methods, the particles in SPH are no longer restricted by grids, and thus the volume of the neighboring particles in support domain of a certain particle cannot be kept constant, especially at moving FSI interfaces. This has great influences on the normalization rule of the kernel function and results in the density oscillation and pressure instability. In multiphase SPH, to adapt to the similar mass discontinuity and density discontinuity issues on a multiphase interface to the FSI interface, a corrected density re-initialization formula was developed by Chen et al. [165] as:

$$\rho_i^{\text{new}} = \frac{\sum_j \rho_j' V_j W_{ij}}{\sum_j V_j W_{ij}}, \tag{31}$$

$$\rho_j' = \frac{(p_j - p_0)}{c_s^2} + \rho_{i0}, \tag{32}$$

where ρ_j' is the density obtained by the pressure of the particle j and the equation of state for the particle i, c_s is the speed of sound, and ρ_{i0} is the reference density of the particle i. The corrections can be regarded as converting particles of different phases into the same phase with the interested particle. To avoid the artificial diffusions and to reduce the computational cost, this equation is often applied after every 20 to 30 time steps. The discontinuities on the multiphase interfaces present great challenges on accurately and stably solving the continuity and momentum equations. To deal with this problem, Hu and Adams [64,166] developed an effective scheme to calculate the pressure gradient,

$$\begin{cases} \left(\frac{1}{\rho}\nabla p\right)_i = \frac{1}{m_i}\sum_j \left(V_i^2 + V_j^2\right)\tilde{p}_{ij}\nabla_i W_{ij}, \\ \tilde{p}_{ij} = \frac{\rho_i p_j + \rho_j p_i}{\rho_i + \rho_j}. \end{cases} \tag{33}$$

This approximation is reasonable for multiphase flows with small density differences. However, for those with large density ratios, the influence of the pressure from neighboring particles may be improperly ignored [165]. To treat the large density ratio, Chen et al. [165] presented an alternative formula based on the assumption of the pressure continuity across the interface. In this approach, all the neighboring particles of other phase in support domain of the interested particle are regarded as the interpolation points with the same phase. Only the position, velocity, volume and pressure of these particles are taken into account when solving the acceleration and density of the central particle. Accordingly, the pressure term in momentum equation is approximated as:

$$\left(\frac{1}{\rho}\nabla p\right)_i = \frac{1}{\rho_i}\sum_j V_j p_j \nabla_i W_{ij}. \tag{34}$$

Besides, Grenier et al. [167] proposed a multiphase flow SPH model to treat the density discontinuity, and this may be regarded as an extension of the work by Colagrossi and Landrini [65]. The authors denoted their method as a so-called Hamiltonian interface SPH formulation. This discretized formula (35) is based on the Shepard kernel [168] for the density evaluation by eq. (36),

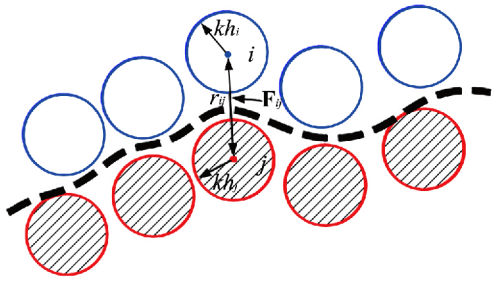

Figure 5 (Color online) An illustration of particle-particle contact.

$$\begin{cases} \rho = \dfrac{1}{\Gamma_i^{\chi}} \sum\limits_{j\in\chi} m_j W_{ij}, \\ \Gamma_i^{\chi} = \sum\limits_{j\in\chi} \dfrac{m_j}{\rho_j} W_{ij},\ i \in \text{fluid}\chi, \end{cases} \tag{35}$$

$$\begin{cases} \nabla f = \sum\limits_{j=1}^{N} \left(\dfrac{f_i}{\Gamma_i} + \dfrac{f_j}{\Gamma_j} \right) \dfrac{m_j}{\rho_j} \nabla_i W_{ij}, \\ \Gamma_i = \sum\limits_{j=1}^{N} \dfrac{m_j}{\rho} W_{ij}. \end{cases} \tag{36}$$

This SPH scheme allows a relatively accurate treatment of the discontinuity of the quantities at the interface (such as the pressure) for the modeling of multiphase flow.

The afore-mentioned algorithms for treating multiphase interface can be extended to the treatment of FSI interfaces. Besides, in FSI problems, the moving FSI interface with a large density discontinuity remains a big problem for applications of SPH in impact and explosion problems. For such cases, the interface between the fluid (an explosive gas) and the structure is also treated as a moving boundary with the particles from two sides of the boundary interacting with each other. Recently, Liu et al. [121,128] proposed a density adaptive algorithm to treat the large density ratio of solid (metal structure) to fluid (explosive gas) around the FSI interface in explosion problems, which is shown as follows. In the SPH method, the density summation approach and the continuity approach [17] are usually used to update the density, and these two formulae can be written as:

$$\dot{\rho}_i = \rho_i \sum_{j=1}^{N} \frac{m_j}{\rho_j} \mathbf{v}_{ij}^{\beta} \cdot \frac{\partial W_{ij}}{\partial \mathbf{x}_i^{\beta}}, \tag{37}$$

$$\dot{\rho}_i = \sum_{j=1}^{N} m_j \mathbf{v}_{ij}^{\beta} \cdot \frac{\partial W_{ij}}{\partial \mathbf{x}_i^{\beta}}. \tag{38}$$

Eq. (37) cannot be exactly satisfied while it is effective and flexible for the simulation of problems with a large density ratio. In contrast, eq. (38) is believed to be more accurate because it is obtained through rigorous mathematical transformations [17]. When using eq. (38), however, the large density discontinuity for the interface particles may lead to numerical oscillations (instability) and further terminate the simulation. By combining these two equations, the time rate of change of density can be approximated by

$$\dot{\rho}_i = \sum_{j=1}^{N} \frac{\rho_i + \psi_i \rho_j}{\rho_j (1+\psi_i)} m_j \mathbf{v}_{ij}^{\beta} \cdot \frac{\partial W_{ij}}{\partial \mathbf{x}_i^{\beta}}. \tag{39}$$

The contributions of eqs. (37) and (38) to the density approximation are controlled through an adaptive function relationship $\psi_i = \psi(k_i) = \dfrac{1}{\ln k_i}$, as shown in Figure 6. The dimensionless variable k_i is defined as $k_i = \rho_{i,\max} / \rho_{i,\min}$, where $\rho_{i,\max}$ and $\rho_{i,\min}$ represent the maximal and minimal density values of the neighboring particles around the particle i, respectively. Therefore, for a multi-materials system, the density of materials can be calculated in an adaptive way when the density ratio of different materials is high.

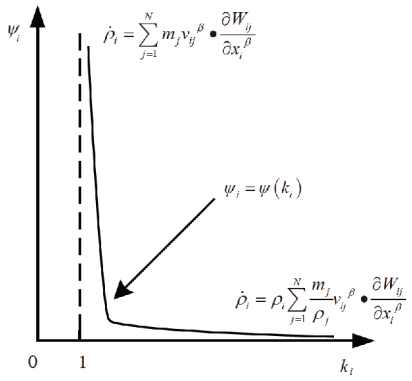

Figure 6 Schematic diagram of the function $\psi_i=\psi(k_i)$.

3.2.3 *Coupled dynamic solid boundary treatment for FSI interface*

For treating the FSI interface as a fixed solid boundary or a moving boundary, there are some drawbacks when using only one type of virtual particles such as repulsive particle or dummy particle, just as mentioned in sect. 3.1. With considerations on both the accuracy and stability of boundary treatments, Liu's group [80,169] developed a coupled dynamic solid boundary treatment algorithm (CD-SBT) for dealing with both the fixed and moving rigid boundaries. In CD-SBT, two types of virtual particles named as the repulsive particles and ghost (or dummy) particles are applied to treat the solid boundary, as shown in Figure 7(a). A soft repulsive particle model was presented in CD-SBT that includes a distance-dependent repulsive force with finite magnitude on the particles approaching solid boundaries, which is given by

$$\mathbf{F}_{ij} = 0.01c^2 \cdot \chi \cdot f(\eta) \cdot \frac{\mathbf{x}_{ij}}{r_{ij}^2}, \tag{40}$$

$$\eta = r_{ij} / (0.75 h_{ij}), \tag{41}$$

$$\chi = 1 - \frac{r_{ij}}{\Delta d},\ 0 < r_{ij} < \Delta d, \tag{42}$$

$$f(\eta) = \begin{cases} 2/3, & 0 < \eta \le 2/3, \\ (2\eta - 1.5\eta^2), & 2/3 < \eta \le 1, \\ 0.5(2-\eta)^2, & 1 < \eta \le 2, \\ 0, & \text{otherwise}, \end{cases} \tag{43}$$

where r is the distance between two SPH particles, and Δd is the initial distance of two adjacent SPH particles. It is known that the Lennard-Jones molecular force is a highly repulsive force which may produce pressure disturbances. Using such soft repulsive force, the CD-SBT can effectively prevent non-physical particle penetration while alleviating the pres-

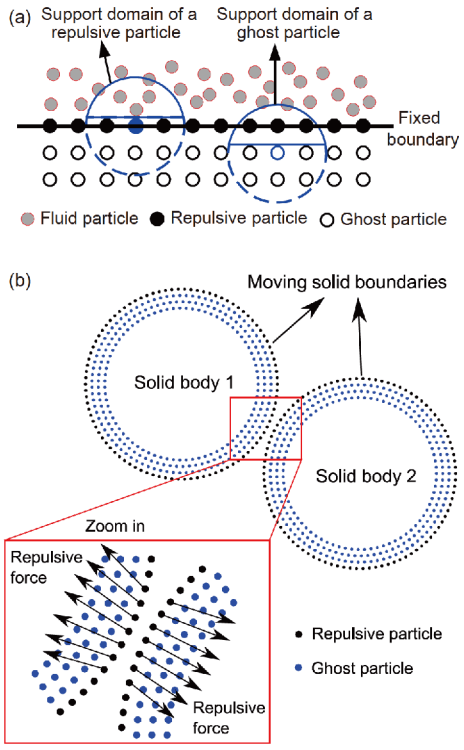

Figure 7 (Color online) Illustration of the CD-SBT algorithm for (a) fixed and (b) moving solid boundaries.

sure disturbances.

The support domains of the fluid particles usually intersect the solid boundary with insufficient neighboring particles that leads to a low accuracy of the simulation at the boundary areas. Therefore, to restore consistency, SPH particle approximation schemes with higher order accuracy (e.g., Shepard filter method, CSPM or FPM) are involved in CD-SBT for approximating virtual particles. That is to say that the variables of the virtual particles can be obtained as:

$$\rho_i = \sum_{j=1}^{N} \rho_j W_{ij}^{\text{new}} \frac{m_j}{\rho_j} = \sum_{j=1}^{N} m_j W_{ij}^{\text{new}}, \tag{44}$$

$$\mathbf{v}_i = \sum_{j=1}^{N} \mathbf{v}_j W_{ij}^{\text{new}} \frac{m_j}{\rho_j}. \tag{45}$$

In this approach, the corrective kernel function W_{ij}^{new} by the improved approximation scheme (e.g., FPM or DFPM) is utilized to obtain the virtual particles variables. This CD-SBT algorithm can be further extended to the treatment of solid-solid interfaces, as shown in Figure 7(b). The virtual SPH particles in this extended CD-SBT can move with the solid objects. Therefore, the implementation of fluid-solid interaction in this article is straightforward and the repulsive force model can effectively prevent the penetration of surfaces of two solid objects in the simulation of FSI problems.

4 SPH coupled with other methods

4.1 SPH coupled with FEM

For modeling FSI problems, some complex algorithms and considerable computational cost are required for Eulerian-based methods to treat the moving boundaries and interfaces. The Lagrangian methods have its natural advantages for capturing moving boundaries in FSI problems. However, when using the Lagrangian grid-based methods such as FEM, the large element distortion may occur and the extreme fluid motion such as the breakup of free surfaces may even limit the use of this kind of methods. Nevertheless, the FEM has been widely employed in modeling problems without extreme element distortions due to its high accuracy, good stability and great efficiency. As a meshfree particle method, SPH has its advantages in dealing with violent FSI problems as the problem of mesh distortion at the interfaces can be naturally avoided and no interface or free surface tracking algorithms are required. Considering both the advantages and drawbacks of these two kinds of Lagrangian methods, FEM and SPH, some researchers have coupled SPH with FEM for modeling FSI problems [136,137,170-172]. In these simulations, the successful application of FEM in solving structural dynamics and the effectiveness of SPH in modeling fluid dynamics are integrated with each other. Since both SPH and FEM have been well developed, the key point of this coupling approach lies in the contact algorithms between these two methods. Here we review the development of different coupling or contact algorithms in detail. As for the nonlinear finite elements formulations, one may refer to ref. [173] for more information.

In the early 1990s, Attaway et al. [174] proposed the coupling of SPH with FEM for modeling structure-structure impact problems and they used an iterative master-slave scheme of contact force to treat coupling. Later different algorithms have been developed based on this kind of master-slave coupling [172,175] that requires the calculation of contact force for preventing the SPH particles from penetrating into the FEM meshes. For example, De Vuyst et al. [176] implement the contact algorithm by considering the FEM nodes as SPH particles. Groenenboom and Cartwright [172] used a non-iterative master-slave scheme to treat the contact force. Zhang et al. [175] also developed a master-slave SPH-FEM coupling algorithm, and we will take this as an example to show how to couple the SPH with FEM using the contact force model. In this article, the SPH particles are attached to the standard finite elements in the interface, as shown in Figure 8. The background particles possess the property of SPH particles while they carry the variables consistent with those of the corresponding FE nodes, e.g., mass, velocity and stress. In this way, the FEM nodes are added to the SPH neighbor list by using the background particles. For example, the particle approximation for the

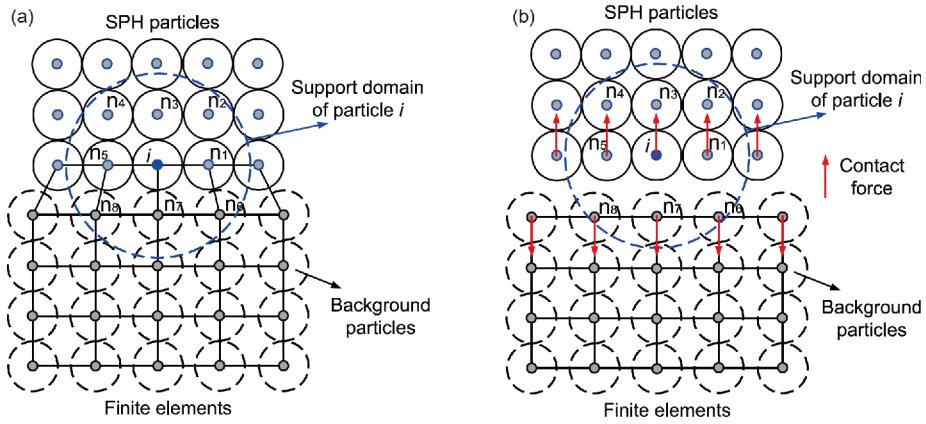

Figure 8 (Color online) (a) The attachment of SPH particles to finite elements and (b) contact force produced between SPH particles and finite elements.

particle i is performed with the contributions from particles n_1 to n_5 and FEM nodes n_6, n_7, n_8 (see Figure 8(a)). Therefore, the boundary truncations for the SPH particles can be effectively avoided. When the SPH particles are very close to the FE nodes, the contact force need to be performed on these particles and nodes. The vector of the contact force can be calculated in the same way as the contact of SPH particle to particle. Then the contact force is given by

$$Q(x_i) = \sum_{j}^{NCONT} \frac{m_j}{\rho_j}\frac{m_i}{\rho_i} Kn \frac{W(r_{ij})^{n-1}}{W(\Delta p_{\text{avg}})^{n}} \nabla_i W(r_{ij}), \tag{46}$$

where *NCONT* denotes the number of neighboring SPH particles for an FEM node i. r_{ij} is the distance between the particles i and j, p_{avg} is the average value of the smoothing length, and K and n are the user-defined parameters.

Recently, the coupling of SPH with FEM without using the master-slave coupling algorithm has been developed by different researchers [136,138,171]. To couple SPH with FEM, Fourey et al. [171] applied the ghost particles scheme to obtain the pressure from the fluid side. In this article, the minoring ghost particles are used to complete the support domain of the kernel of particles approaching the boundary. Then the pressure on the solid boundary acting by the SPH particles can be obtained by

$$p_{\text{boundary}} = \frac{1}{N}\sum_{i=1}^{N} p_i, \tag{47}$$

where N denotes the number of sampling particles close to the boundary and P_i is the pressure of a sampling particle i.

Considering that no shear stress can be exerted on the structure by the fluid particles, Long et al. [136] developed a novel coupling algorithm based on the ghost particle scheme to treat complex geometry boundaries. In their work, the kernel support domain of a fluid particle approaching the boundary can be divided into subareas that are used to generate the corresponding ghost particles, as shown in Figure 9. The forces from the FEM structure to the SPH fluid

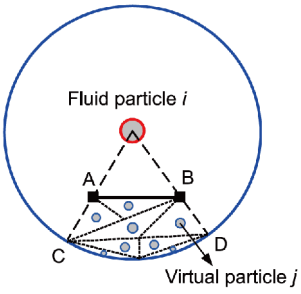

Figure 9 (Color online) The subarea ABCD and corresponding ghost particles in support domain of fluid particle i.

particles can be calculated directly through the ghost particles. To maintain the conservation of momentum equation, the opposite forces of ghost particles to fluid particles are also applied on the structure. Taking one subarea of the boundary for example (see Figure 9), the AB belongs to a segment of the boundary in support domain of a fluid particle i, and a subarea ABCD along with the corresponding ghost particles are generated for calculating fluid-structure interactions. The force exerted from the ghost particle j to the fluid particle i is denoted as $\mathbf{F}_{G_j tF_i}$ and then the force from the segment AB to the fluid particle i can be obtained as:

$$\begin{aligned}\mathbf{F}_{S_{AB}tF_i} &= \sum_{j\in ABCD} \mathbf{F}_{G_j tF_i} \\ &= m_i\Bigg[-\sum_{j\in ABCD} m_j\left(\frac{p_i}{\rho_i^2}+\frac{p_j}{\rho_j^2}\right)\nabla_i W_{ij} \\ &\quad + \sum_{j\in ABCD}\frac{4m_j(\mu_i+\mu_j)\mathbf{x}_{ij}\cdot\nabla_i W_{ij}}{(\rho_i+\rho_j)^2(\mathbf{x}_{ij}^2+\eta^2)}\mathbf{v}_{ij}\Bigg].\end{aligned} \tag{48}$$

This equation is just one way to calculate the viscous force that can also be computed with other forms. Similarly, the force from the fluid particle to the segment AB is given by $\mathbf{F}_{F_i tS_{AB}} = -\mathbf{F}_{S_{AB}tF_i}$ and the force on nodes A and B should be

$\mathbf{F}_{F_i tS_{AB}} / 2$.

Furthermore, some other coupling techniques have also been developed. For example, Yang et al. [138] used the Monaghan boundary condition to treat the coupling of SPH with FEM. Li et al. [137,170] developed the so-called interface-energy-conserving coupling strategy for transient fluid-structure interaction, and with this strategy neither numerical energy injection nor dissipation occurs at the interface during the simulation process. It is clear that these coupling algorithms have some advantages for treating the coupling interface and a comprehensive coupling algorithm with good performance in accuracy, stability and efficiency is desirable.

4.2 SPH coupled with FVM

Grid-based methods like FVM have many advantages in modeling fluid flow with large fluid domain due to their good robustness and high efficiency. However, they may meet some difficulties for dealing with geometrically complex domains requiring high-quality meshing, moving fluid-solid interfaces and free surface flows. The use of unstructured grids and techniques like the immersed boundary method (IBM) [177,178] can be an effective way to solve these problems. However, in order to deal with extremely complex free surface flows, it is still very difficult for such grid-based methods to achieve accurate and stable solutions. In contrast, due to its Lagrangian and meshfree characteristics, SPH is very suitable for dealing with these serious challenges that the grid-based methods like FVM faced. However, the computational effort of SPH is comparatively high and it is not straightforward to treat solid boundaries. Therefore, the combination of SPH with other grid-based methods is very attractive and the advantages of two methods can be explored. For such purpose, the grid-based methods such as FVM or FDM may be applied in a larger fluid domain, whereas the SPH method can be used in local regions with geometrically complex domains, moving interfaces or free surfaces. As the efficient CFD methods like FVM are usually based on the Eulerian grid while the SPH is a Lagrangian particle method, there exists many difficulties in coupling these two kinds of methods together.

Recently, Neuhauser and Marongiu [179] proposed the coupling of SPH with FVM for treating boundary layers near hydrofoils. Napoli et al. [180] further developed a coupled FV-SPH method for incompressible flows. In this method, a layer of grid cells is located in the SPH domain, and a band of virtual particles is placed in the FVM domain (both near the interface). The hydrodynamics variables can thus be calculated using the suitable interpolation procedures from the local solutions. In this manner, a smooth transition between the solutions in the FVM and SPH is obtained. Then this method has successfully been applied to model viscous flows and wave processes. However, no violent FSI with breaking free surfaces is involved in their simulations, and this method shows a promising performance in modeling violent FSI that could demonstrate larger advantages of such a coupling approach.

Marrone et al. [133] also developed a SPH-FVM coupling algorithm, and further applied it to model free surface flows. Similarly, the local region with free surfaces is modeled by SPH, whereas the FVM is applied to solve the bulk flow in a larger region and the wall regions. The overlapping zones are utilized to guarantee the continuity between these two solutions. This method is practically applied to model fluid flows with breaking free surfaces, which shows the superiority of these two methods both in accuracy of local regions and efficiency. However, as mentioned in ref. [134], this method does not allow the relevant mass transfer and/or free surface crossing between the two subdomains, which limits its practical applications to engineering problems. Because, in practical applications, the position and extension of free surface deformation and transferred vorticity are not easily determined. To deal with this problem, Chiron et al. [134] further extended this coupling method to make it possible for mass transfer between the SPH and FVM sub-domains and for the free surface crossing the overlapping region. The extended coupling method involves a technique for creating and deleting particles in SPH and an improved technique for free surface prediction in FVM using the information recovered from the SPH solver. This coupling method has been successfully applied to violent FSI problems (liquid sloshing) where vorticity and free surface significantly pass from one domain to the other.

Different from above coupling works where both SPH and FVM are used for modeling fluid flows, Chen et al. [181] also coupled SPH with FVM for the simulation of fluid-particle interaction problems. In this article, SPH is applied for the discrete phase to capture the movement of each individual particle due to its Lagrangian and particle feature. FVM is used for the continue phase to compute the turbulent fluid due to its grid-based feature. By using the pseudo-fluid model, the fluid and solid phases are coupled through the effects of drag force, gas pressure and volume fraction of each phase. Based on this approach, Chen et al. [182] further developed a SDPH-FVM coupling method for modeling fluid (gas)-particles multiphase flows. The so-called SDPH (smoothed discrete particle hydrodynamics) is a developed SPH that is more suitable for describing the particle characteristics. Taking advantages of SPH for discrete particles and FVM for fluid flows, this kind of coupled method exhibits good efficiency and accuracy in modeling fluid-particle interactions. However, just as mentioned in ref. [181], the constitutive model of a pseudo fluid is still under development, and the boundary treatment should also be deeply studied.

4.3 SPH coupled with EBG

The EBG technique can also be regarded as a particle method. It was first proposed for the simulation of membrane structures (or named elastic shells [183]), and was later developed to model the red blood cell (RBC) membranes [184,185]. The flexible structure can also be considered as a membrane structure, and hence the EBG is very attractive for modeling the movement and deformation of flexible structures. With the coupling of SPH and EBG, it is possible to model the fluid-flexible structure interaction, in which the viscous fluid flow governed by Navier-Stokes equations is modeled by SPH, and the dynamic movement and deformation of flexible fibers are modeled through EBG. The SPH-EBG coupling method was originally proposed by Hosseini and Feng [185] to model the deformations of RBC in shear flows, and later Yang et al. [142-144] extended the SPH-EBG coupling method to the simulation of fluid-flexible fiber interactions with good results achieved. In this section, the EBG method will be briefly introduced and the coupling of SPH with EBG will be addressed in detail.

4.3.1 EBG model for flexible structure

In EBG model, the flexible structure is discretized into particles that can interact with each other and with fluid (SPH) particles as well. As shown in Figure 10, an EBG is composed of two adjacent line segments connecting three neighboring particles, and the bending moment in flexible structure can be transformed to the pairs of forces acting on the particles. Based on the Newton's second law of motion, the governing equation for a flexible body particle is given by

$$m\frac{\mathrm{d}v}{\mathrm{d}t}=\mathbf{T}+\mathbf{F}^{B}+\mathbf{F}^{D}+\mathbf{g}, \tag{49}$$

where $\mathbf{T}$ represents the tension acting on a EBG particle (flexible body) from adjacent EBG particles, $\mathbf{F}^{B}$ denotes the force due to EBG bending moment, and $\mathbf{F}^{D}$ stands for the fluid force acting on a EBG particle from the neighboring fluid SPH particles. The tension can be calculated as:

$$\mathbf{T}_{ba}=EA\left(\frac{r_{ba}}{r_{ab}^{0}}-1\right)\frac{\mathbf{r}_{ba}}{r_{ba}}, \tag{50}$$

where E and A denote the Young's modulus and the cross-sectional area of the fiber, respectively. r_{ab}^{0} represents the reference distance between particles a and b. The force $\mathbf{F}_{ab}^{B}$ acting on particle b from particle a can be calculated by

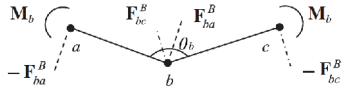

Figure 10 Illustration of the EBG model. An EBG is composed of two adjacent line segments connecting three neighboring particles.

$$\mathbf{F}_{ba}^{B}=\frac{\mathbf{M}_b\times\mathbf{r}_{ba}}{r_{ab}^{2}}, \tag{51}$$

where $\mathbf{M}_b$ denotes the moment acting on particle b (see Figure 10), and it is defined as:

$$M_b=\frac{EI(\theta_b-\theta_b^{0})}{r_{ba}+r_{bc}}, \tag{52}$$

where EI is the bending rigidity, θ denotes the deflection of the flexible fiber, and θ_b^{0} is the reference deflection at particle b. The direction of $\mathbf{M}_b$ is determined by the value of $\theta_b-\theta_b^{0}$, i.e., it is clockwise if $\theta_b-\theta_b^{0}$ and counterclockwise if $\theta_b-\theta_b^{0}$.

4.3.2 SPH-EBG coupling algorithm

For modeling the fluid-flexible structure interaction, it is natural to couple SPH with EGB through allowing the interaction of neighboring fluid and flexible structure particles. That is to say the particles of flexible structure can be regarded as moving boundaries of the fluid SPH particles, and the fluid SPH particles and structure EBG particles are treated as neighboring particles. In this way, it is convenient to include the structure particles in discretized governing equations when calculating forces acting on fluid particles. The force on the flexible structure particles from the neighboring fluid particles can be calculated similarly except that the direction of the force is the opposite, which is given by

$$\mathbf{F}_{ba}^{D}=m_a\left(\frac{p_a}{\rho_a^{2}}+\frac{p_b}{\rho_b^{2}}\right)\cdot\nabla_b W_{ba} -\frac{m_a(\mu_a+\mu_b)\mathbf{r}_{ab}\cdot\nabla_b W_{ba}}{\rho_a\rho_b(r_{ab}^{2}+0.01h^{2})}\mathbf{v}_{ba}, \tag{53}$$

where a and b denote the fluid SPH and structure EBG particles, respectively. The dynamic viscosity of the EBG particle b is the same as that of the SPH particle a. The pressure of the EBG particle b can be obtained as:

$$p_b=\sum_a p_b W_{ba}\frac{m_a}{\rho_a}\Big/\sum_a W_{ba}\frac{m_a}{\rho_a}, \tag{54}$$

where the summation is over all neighboring fluid particles of the EBG particle b. The total fluid force on the EBG particle b is

$$\mathbf{F}_b^{D}=\sum_a\mathbf{F}_{ba}^{D}. \tag{55}$$

It is noticed that there are different ways to calculate the viscosity force, and here we just give only one typical (equation 53). Through this, the EBG particles can interact with each other by taking account of the tension and bending forces, and they can also interact with fluid particles by considering the interaction forces between fluids and flexible structure.

For the coupling of SPH with EBG, the match of time integration in these two methods is a challenging work, as the time step for EBG may be less than the time step for SPH

time integration. One way to deal with this problem is to keep the time integration of EBG nested in SPH time integration. To explain it further, during the inner loop of EBG integration, the SPH particles keep static and the force on EBG particles due to SPH particles remains the same. Also, the EBG particles cannot penetrate their neighboring SPH particles during this inner loop of the integration process. Actually, the time of one entire inner loop for EBG integration should be the same as that of one time-step in SPH.

4.4 SPH coupled with other methods

As a Lagrangian particle method, SPH has many advantages over conventional grid-based methods, especially for modeling violent FSI problems. Nevertheless, it also has some drawbacks due to its Lagrangian and meshfree features. Fortunately, many of these drawbacks can be removed by the coupling of SPH with other methods. For example, in modeling of the solid mechanics problems the stress instability and inaccurate stress or strain are usually produced by SPH. The coupling of SPH with FEM can be an efficient way to deal with this problem, in which the large deformation areas or fluid areas are modeled by SPH while the other structure areas are modeled by FEM. The SPH is also often restricted to model relatively small problem domain due to its expensive computational cost. To treat this problem, the coupling of SPH with FVM has been developed rapidly during these years, and in this coupling the larger fluid region can be simulated by FVM, and the SPH is only applied in the local region showing strong nonlinear dynamics behavior. Besides, to model the interactions of fluids with a flexible structure or thin-walled structure, the coupling of SPH with EBG can be more attractive as the thin walled structure is difficult to simulate accurately by SPH due to its boundary deficiency problem.

Besides the coupling of SPH with FEM, FVM and EBG, there are some popular methods that can be efficiently combined with SPH for different applications, such as coupling SPH with DEM [139-141]. DEM is initially proposed to investigate the discontinuous mechanical effects where the solid is composed of particles at meso-scale, and then it has been widely applied to study large deformations, fracture and failure of materials [141]. In DEM, the contact model between particles is used to treat the mechanical behavior of materials. The contact model is usually composed of many mechanical elements, e.g., a spring and a dashpot in both the normal and shear directions. Then, the contact forces can be obtained by the force-displacement law according to the relative displacements between particles. The velocity and position of a particle is determined by the obtained contact force before. To model the fracture and failure of materials, the normal tensile strength and frictional strength are determined, and the contact between particles can be broken when the contact force exceeds the strength. Therefore, considering the advantages of DEM, the coupling of SPH with DEM has many superiorities for solving FSI with many rigid bodies or with structural deformation and failure.

Utilizing the aforementioned two superiorities of SPH-DEM coupling method, many researchers developed different coupling models for various FSI problems. Cleary [186] coupled DEM and SPH to predict the motion of the solid particles in a slurry flow. In this work, DEM is used to model the motion of the coarser particulates while SPH is applied to treat the slurry consisting of water and finer particulates. Ren et al. [187] developed a SPH-DEM model to study the wave-structure interaction on a slope. In this work, the SPH combined with a Riemann solver is used to calculate the hydrodynamic loads on the discrete blocks, whereas a multi-sphere DEM is applied to model the movement of the solids under wave attacking. Robinson et al. [188] developed a SPH-DEM coupled method for simulating the sedimentation of granular assemblies with various porosities. In above SPH-DEM models, the solid particles are regarded as a cohesionless granular material. Recently, some SPH-DEM models considering the bond strength between particles have been addressed, and these models have been successfully applied to FSI problems with large solid deformation and solid fracture [6]. For example, Wu et al. [139] developed a coupled SPH-DEM model for FSI problems with free-surface and structural failure. In this work, the fluid flow is modeled by SPH and a parallel bond model is integrated in DEM to represent the real solid structure. Tang et al. [141] developed a coupling method of ISPH and DEM, which can reasonably describe the features of solid movement, deformation, and failure in FSI problems.

Recently, SPH coupling with some other methods has also been addressed. For example, Zhang et al. [189] coupled the boundary element method (BEM) with SPH for the transient fluid-structure interaction and applications in underwater impacts. Being different from the common coupling approaches (SPH for fluid and other method for structure), the structure in this SPH-BEM model is simulated by SPH while the fluid field is solved by BEM. Because the shell structure can be discretized with only a small number of particles while the meshfree and Lagrangian feature of SPH makes it suitable for dealing with the nonlinear problems of structural responses. Meanwhile, the employment of the boundary element also reduces the cost for solving the flow field.

5 SPH modeling of FSI problems

5.1 SPH modeling of FSI problems with rigid structures

Fluid-rigid structure interactions widely exist in natural phenomena and engineering applications, e.g., wave impact

or interaction with structures, water filling and water discharge (to and from a water tank or reservoir), and liquid sloshing etc. Due to its Lagrangian and particle features, SPH can naturally capture the changing and breakup of free surfaces, and violent fluid-structure interactions. Therefore, a large number of studies have been reported in SPH modeling of FSI problems with rigid structures [132,190-193].

Liquid sloshing, if ignoring the deformation of the container, is a typical fluid-rigid structure interaction problem. Shao et al. [11,194] presented an improved SPH method for modeling liquid sloshing in which the kernel gradient correction technique, a coupled dynamic solid boundary treatment and the RANS turbulence model are incorporated. Zhang and Liu [79] developed the DFPM approach and further applied it to simulate liquid sloshing with satisfactory results obtained. In this section, the liquid sloshing due to the pitching motion of a rectangular tank and the water exit simulated using the improved SPH by Shao et al. [11,194], and the liquid sloshing due to the horizontal motion of a rectangular tank simulated using the DFPM by Zhang and Liu [79], are provided as demonstrative examples in SPH modeling of FSI problems with rigid structures.

In the first case, the tank is allowed to rotate around the transverse axis, and hence the pitching motion of a rectangular tank is studied. The external excitation can be described as $\theta = \theta_0 \sin(\omega_r t + \xi_0)$, where θ_0 represents the angular displacement, ω_r is the circular frequency of the pitch motion, and ξ_0 denotes the initial phase. Figure 11 shows the particle distribution due to the pitching motion of a rectangular tank [11]. It is clearly seen that the typical flow dynamics associated with the changing and breaking free surfaces can be well reproduced by the SPH method. Besides, the pressure values on the right wall of the tank are also recorded. Figure 12 shows the pressure values at two probes on the right wall during the sloshing process. It is seen that with the movement of the water tank, the measured pressure values rise and fall periodically. The obtained SPH results agree in general with the results provided by Akyildiz and Erdem [195], who used a VOF model to track the free surfaces. This reveals that the improved SPH method with kernel gradient and CD-SBT algorithm are effective in resolving pressure field, and in treating solid boundaries.

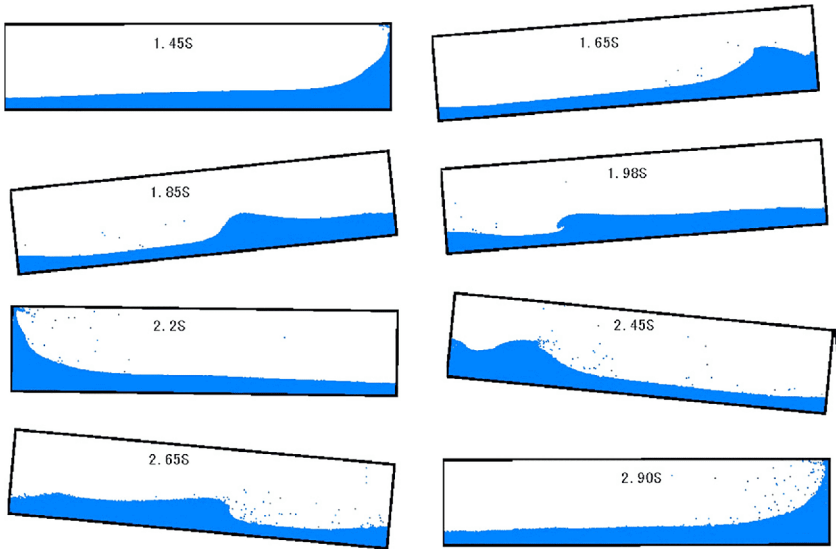

Figure 11 (Color online) Particle distributions at different time instants of the liquid sloshing.

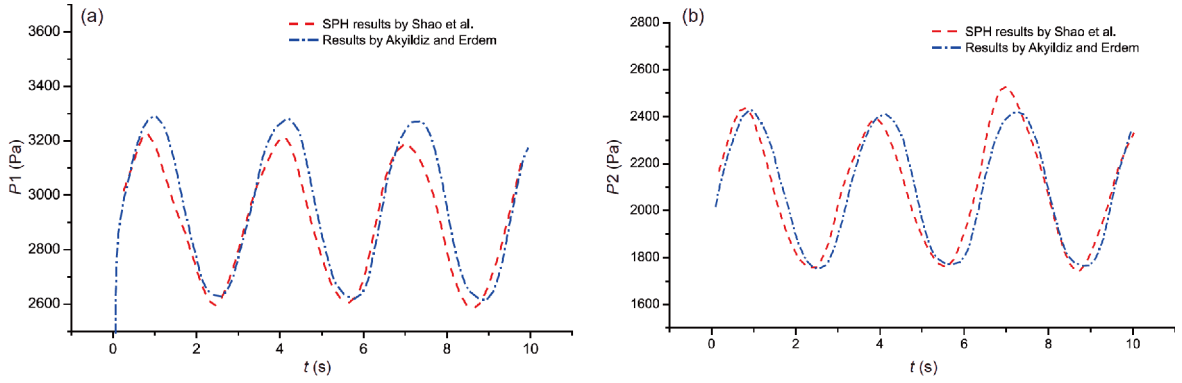

Figure 12 (Color online) Pressure values at probe P1 (a) and P2 (b) during the sloshing process.

The liquid sloshing for the second case [79] undergoes a horizontal external excitation, and the water tank moves according to $S = A\cos(2\pi t / T)$, where S is the horizontal location of the tank, and T is the period of the external excitation. The wave height near the left wall of the tank is tracked for comparison. Figure 13 shows the flow pattern of the sloshing at eight typical time instants within one period. It is shown that during the sloshing process, the maximum pressure region moves as the fluid moves and the uniform pressure distribution can be obtained. For comparison with experimental observations, larger and smaller sloshing frequencies are adopted with h_w=0.6 m, T=1.3 s, and h_w=0.5 m, T=1.875 s. Figure 14(a) shows the wave heights at the probe point obtained by the DFPM simulation and experiment [196] over 20 s course (T=1.3 s). The results from the DFPM simulation agree well with the experimental observations, not only in the pattern, but also for the period and amplitude. The same conclusion can be drawn at a smaller sloshing frequency (T=1.875 s), as shown in Figure 14(b). It is demonstrated that DFPM is an effective method with high

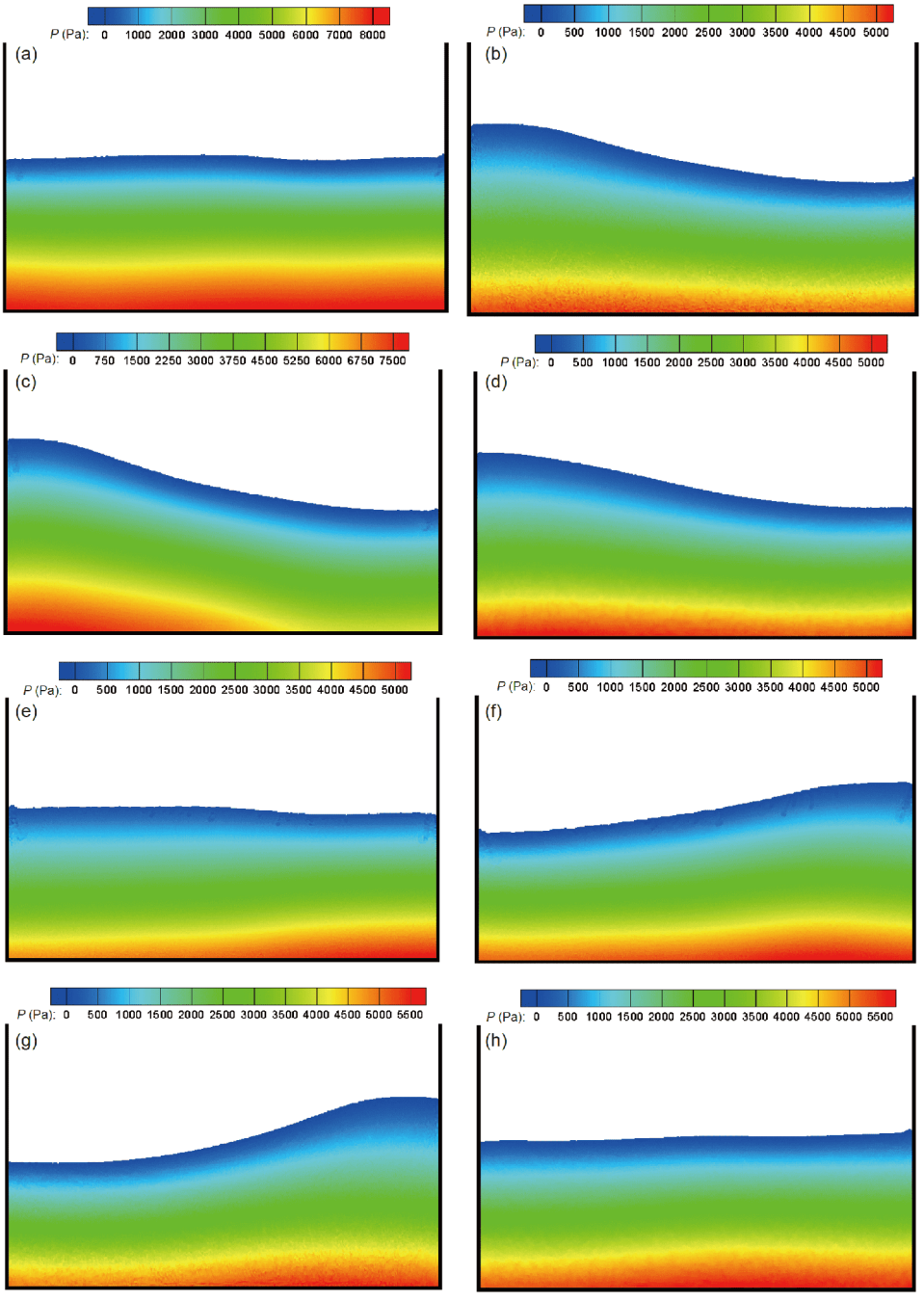

Figure 13 (Color online) Pressure distribution for the liquid sloshing at simulation time t=2.2, 2.4, 2.5, 2.7, 2.9, 3.1, 3.3 and 3.6 s from (a) to (h), respectively.

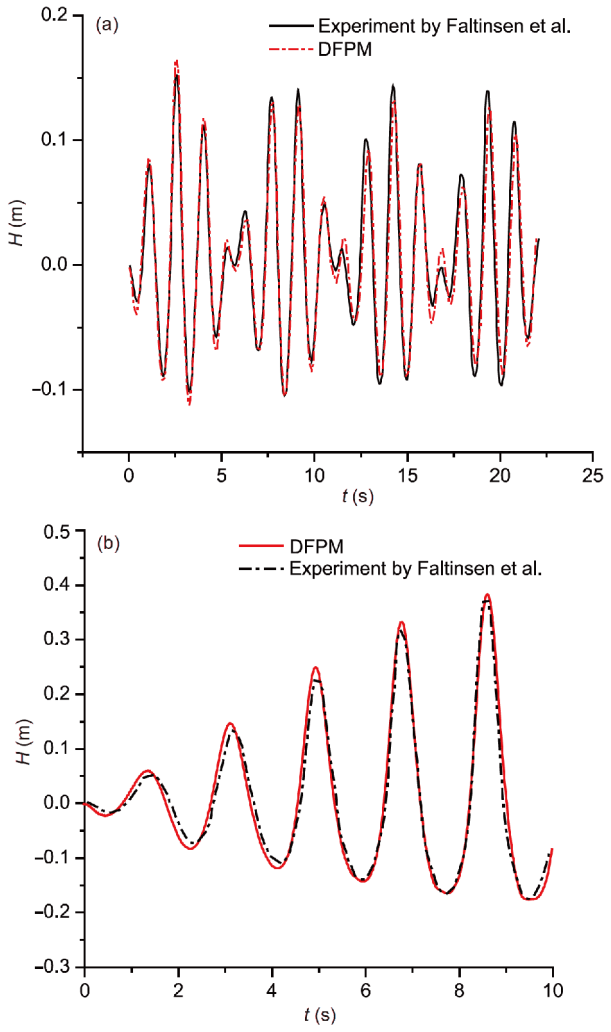

Figure 14 (Color online) Wave height at the probe point for liquid sloshing, (a) h_w=0.6 m and T=1.3 s and (b) h_w=0.5 m and T=1.875 s.

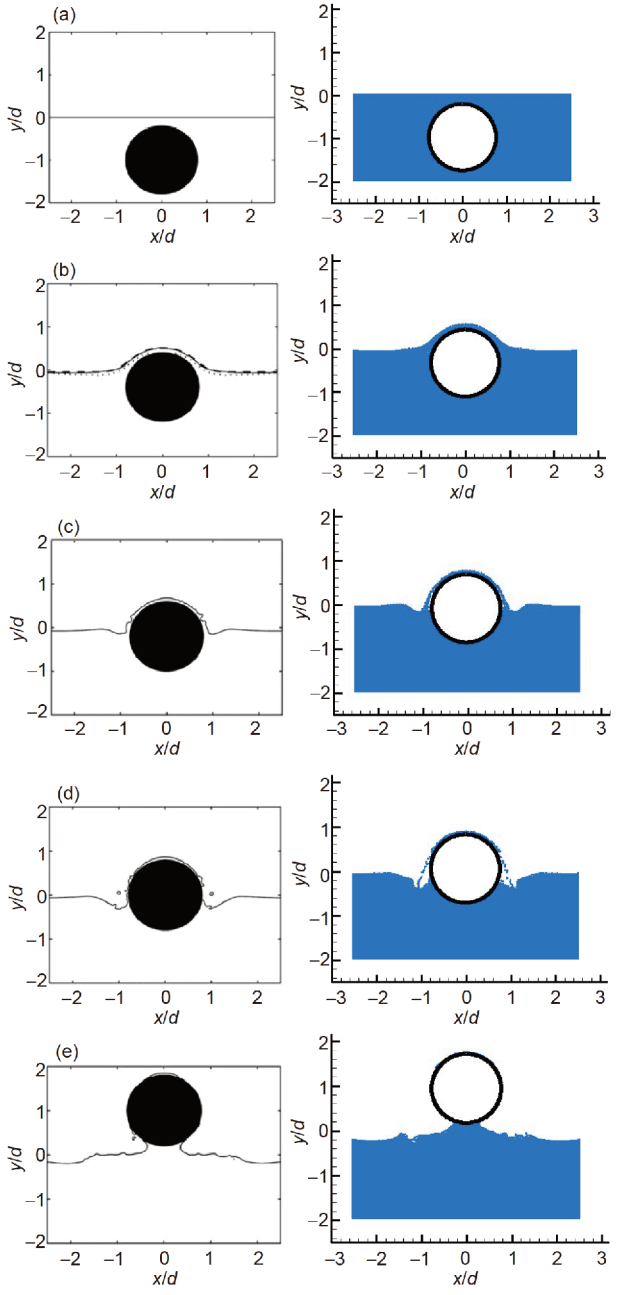

Figure 15 (Color online) The water exit of a horizontal cylinder at different time instants (from (a) to (e): T=0.0, 0.6, 0.8, 1.0, 2.0 s) obtained from left: numerical results by Lin (solid line) [198], numerical results by Greenhow and Moyo (dashed line) [197], theoretical results by Tyvand and Miloh (dotted line) [199] and right: SPH results by Liu et al. [1].

accuracy and stability for modeling fluid-rigid structure interactions.

In the studies carried out by Liu et al. [1] (denoted by the SPH results), the water exit of a horizontal cylinder has been simulated. As shown in Figure 15, the snapshots of the SPH results for this problem along with the existing numerical and theoretical results are plotted for making a comparison. It can be seen that the SPH results are in good agreement with the existing numerical results [197,198] and have a very little deviation with the theoretical results [199]. This deviation is acceptable as the thin fluid layer at the top of the cylinder begins to breakup, and the nonlinear fluid dynamics makes the theoretical results not very reliable. Due to this reason, the theoretical results are not given after T=0.6. From the whole process of this water exit problem, it is clearly seen that not only the free surface morphology and position of the horizontal cylinder before its exit from water are well reproduced, but also the water detachment, breakup, splash and wave generation during the exit of the cylinder from water can be well predicted. It is therefore concluded that the SPH method is very efficient for modeling violent fluid-rigid structure interactions with moving interfaces and free surfaces.

5.2 SPH modeling of FSI problems with elastic structures

Violent free surface flows with strong fluid-solid interactions

can produce a tremendous pressure load on structures, resulting in elastic and even plastic deformations. The fluid-elastic structure interaction is an important issue of FSI problems, and effectively modeling hydro-elastic problems is very important for the applications of SPH in different fields such as ocean engineering. A lot of researches have been reported on SPH modeling of fluid-elastic structure interactions. For example, Oger et al. [200] developed a parallel SPH model for modeling hydro-elastic problems, where the stress instability can be effectively alleviated. Liu et al. [116] developed an improved SPH with KGC technique and the so-called CD-SBT algorithm to deal with the elastic structure in hydro-elastic problems. Antoci et al. [201] presented a SPH-based FSI solver where the assumption of inviscid flow was adopted for fluid dynamics, and the solid dynamics was handled through an incremental hypoelastic relation. In the context of projection-based methods, Hwang et al. [202] developed a projection-based MPS model for fluid-elastic structure interactions. Rafiee and Thiagarajan [115] proposed an improved ISPH method for this problem, in which the PPE was explicitly solved using a simple scheme and an artificial stress term was integrated to alleviate the possible numerical instability. Recently, some coupled methods have also been proposed for fluid-elastic structure interactions. For example, Hu et al. [135,136] developed a FEM-SPH coupled method where the FEM is used to model elastic structure and the SPH is applied to model fluid flow. Khayyer et al. [203] also proposed a coupled method, ISPH-SPH, for the simulation of incompressible fluid-elastic structure interactions.

Here we provide two demonstrative examples of the fluid-elastic structure interactions. The first one involves the dam break with an elastic gate. In this case, an elastic plate is placed at the exit and the water pressure from the dam break results in the deformation of the elastic plate. Liu et al. [116] developed an improved SPH for modeling this problem. The simulation results and the corresponding experimental observations are shown in Figure 16. It is seen that the SPH simulations could accurately reproduce this dam break process including the deformation of the elastic gate and the collapse of the water column. Figure 17(a) and (c) show the horizontal and vertical displacements of the free end of the elastic gate, respectively. Figure 17(c) shows the comparison of the water level between the SPH simulation results and the experimental observations. It is obviously seen that for both the displacements of elastic gate and water height, the SPH results are in great agreement with the experimental observations [201].

For modeling the fluid-elastic structure interactions, the coupling of SPH with FEM can be an attractive approach. Many research studies have been addressed on SPH-FEM modeling of such FSI problems [41,135,137]. Here, we developed a coupling strategy of FEM and SPH and successfully applied it for modeling the water entry with an elastic beam. Figure 18 shows the pressure field in fluid and the stress distribution in elastic beam during the water entry process obtained by the present SPH-FEM. Figure 19 shows the comparison of the vertical force on the beam between results from different sources. The reference solution is obtained by Scolan [204] based on a Wagner model for the fluid

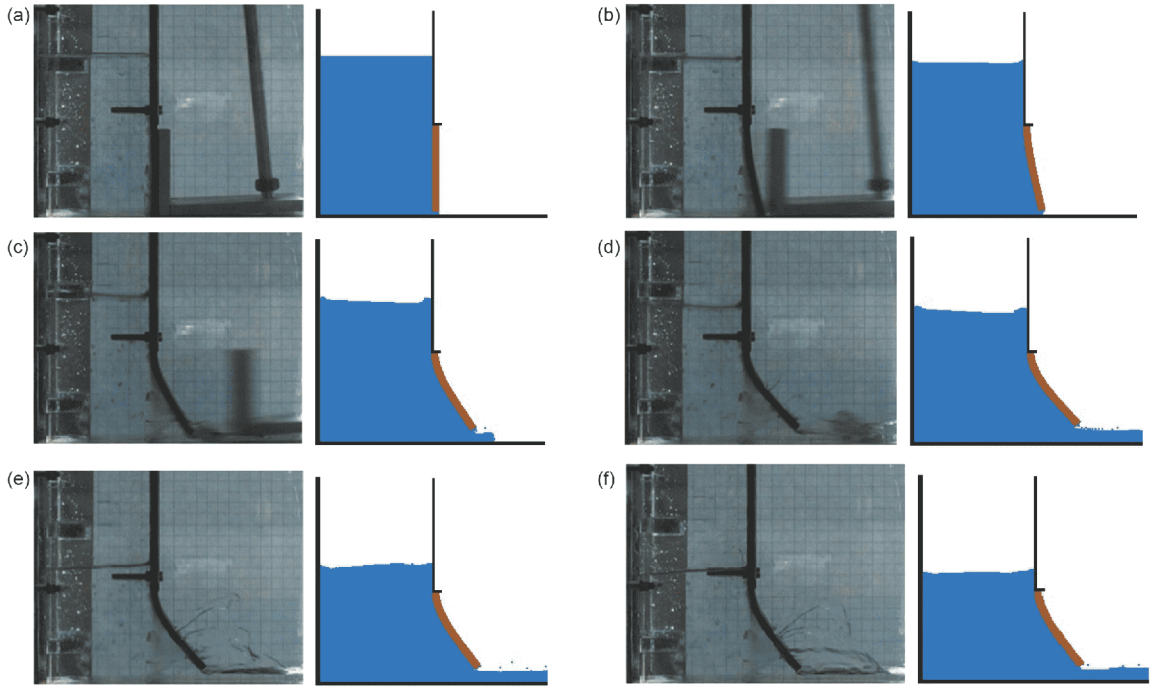

Figure 16 (Color online) SPH simulation snapshots [116] and experimental observations [201] for the dam break with an elastic gate. (a) T=0.0 s; (b) T=0.04 s; (c) T=0.08 s; (d) T=0.12 s; (e) T=0.24 s; (f) T=0.32 s.

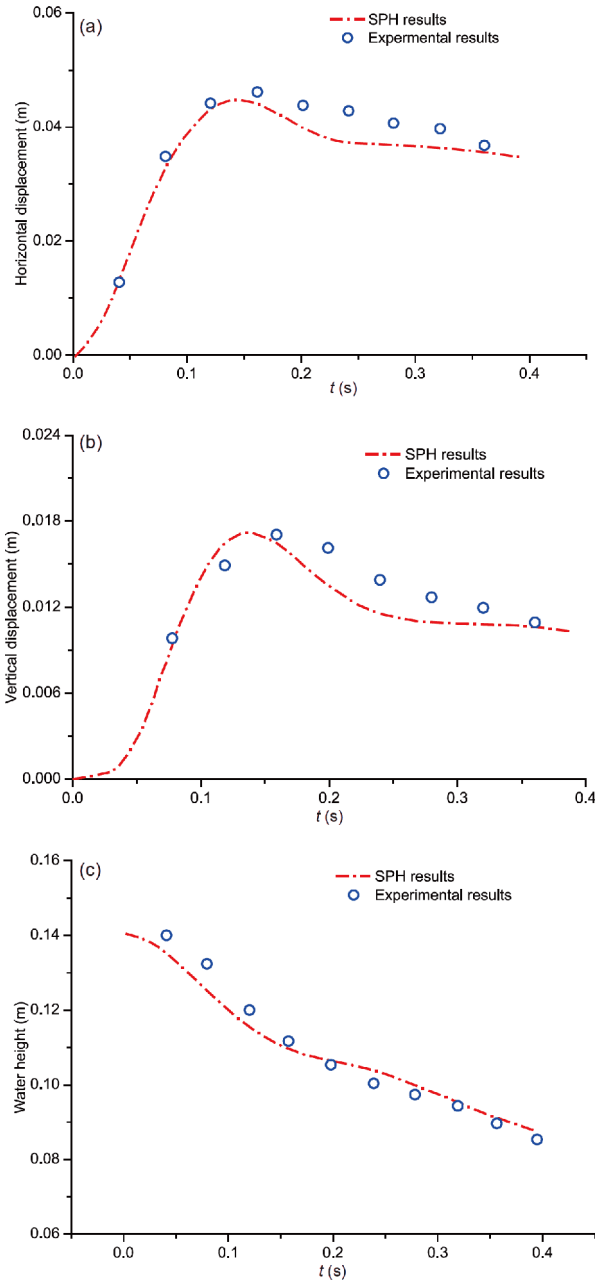

Figure 17 (Color online) Horizontal (a) and vertical (b) displacements of the free end of the elastic gate, and (c) time history of water level during the dam break process, obtained from SPH simulations [116] and experimental observations [201].

coupled to a linear elastic model for the beam. The results by Fourey et al. [171] are also obtained with a SPH-FEM coupling method. It is seen that as the beam experiences a larger deformation with its impacting on the fluid, the smoothed pressure distribution as well as the jet formation can be obtained by the SPH-FEM solutions. The present SPH-FEM can obtain the vertical force on the beam that is very close to the reference semi-analytical solution [204] and other numerical results [171]. This test shows the good performance of the coupling method for modeling violent FSI problem with breaking of fluid surface and deformation of structure well captured.

5.3 SPH modeling of FSI problems with flexible structures

The fluid-flexible structure interactions are very common in natural phenomena and industries. The botany and some animals can adjust the fluid forces imposed on them by changing their shapes or postures. For example, a fish can reduce the fluid drag by its wavy motion while extracting energy from the surrounding vortices [205,206], and a plant can reduce fluid drag by its reconfiguration [207,208]. Since the shape of the flexible structures changes with the fluid field around the corresponding object, the dynamics and flow patterns of the interactions of flexible structures and fluids are much more complex than interactions of rigid structures and fluids. A number of experimental, theoretical and numerical studies have been reported on the dynamics of flexible structures interacting with fluid flows. In Vogel's work [207], the fluid drag and reconfiguration of broad leaves in high winds were investigated by an experimental approach. Gosselin et al. [208] experimentally investigated the reduction of drag on two flexible plates of different shapes in air. Through experimental and numerical approaches, Alben et al. [209,210] studied the drag reduction of a flexible fiber immersed in a soap film. Recently, due to the advantages of SPH in treating moving boundaries and interfaces, some researchers successfully coupled SPH with other methods for modeling fluid-flexible structure interactions. Hu et al. [211,212] simulated the dynamics of a rigid-flexible multibody system in compressible fluid by the coupling of SPH with the absolute nodal coordinate formulation (ANCF) approach, in which the SPH method is used to model the compressible fluid and the ANCF is applied to model the flexible structures. Yang et al. [142-144] developed a SPH-EBG coupling method for the simulation of fluid-flexible structure interaction problems. In this method, the viscous fluid flow governed by the Navier-Stokes equations is modeled by SPH, and the dynamics and deformations of flexible structures are simulated by EBG.

We first review the works by Yang et al. [143] in which a SPH-EBG coupling method was developed for modeling fluid-flexible fiber interactions. In this case, the flow past a fiber with its middle part fixed in the domain is simulated to make a comparison with the experimental results given by Alben et al. [209]. This case involves frequent generation and shedding of vortices at different scales that result in the fluctuations of flow together with oscillations of the flexible fiber. The SPH-EBG simulation results also experience some oscillations, and therefore the numerical data of the fluid drag are smoothed in order to remove the noise for comparison with the experimental observations. Figure 20 shows

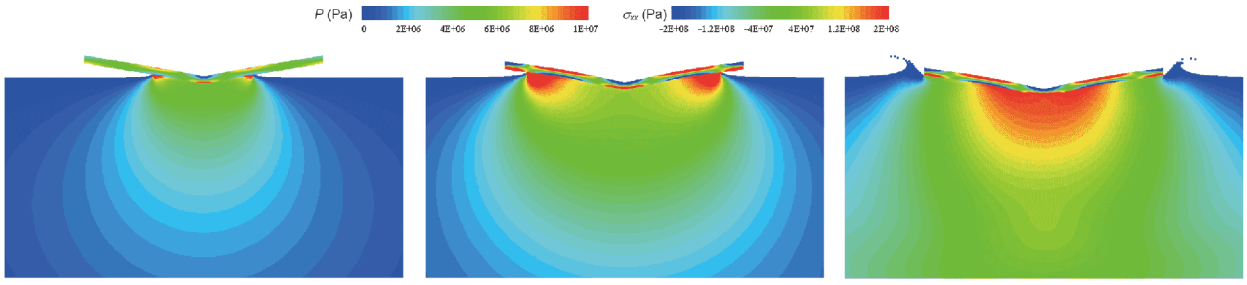

Figure 18 (Color online) The stress distribution in elastic beam and the pressure field in fluid during the water entry process obtained using present SPH-FEM. From left to right, the simulation time is 1, 2 and 3 ms, respectively.

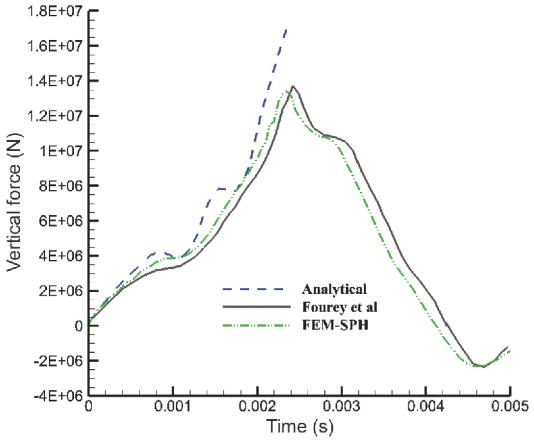

Figure 19 (Color online) Time history of the vertical force on the beam obtained from present SPH-FEM, the semi-analytical solution [204] and the SPH-FEM results by Fourey et al. [171].

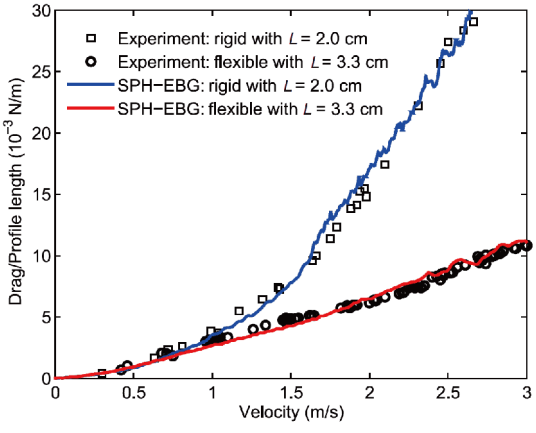

Figure 20 (Color online) Comparison of SPH-EBG results [143] with the experimental results from Alben et al. [209]. The length of the rigid fiber is 2.0 cm and the length of the flexible fiber is 3.3 cm.

the variation of the fluid drag per unit profile length versus the flow velocity. It is seen that the SPH-EBG simulation results are in good agreement with the experimental results for both the rigid and flexible fibers. It is therefore demonstrated that the SPH-EBG coupling method is very effective in modeling fluid-flexible interaction problems.

According to the SPH-EBG simulation results, three typical bending modes of flexible fibers during the fluid-flexible fiber interaction process are identified, i.e., the U-shaped mode, the flapping mode, and the closed mode (see Figure 21). With the flow velocity increasing from zero, the fiber undergoes more bending and is folded with a stable U shape (Figure 21(a)). With a further increase in the flow velocity before it reaches a critical value, the two ends of the flexible fiber begin to swing due to the occurrence of vortex shedding, which may produce a number of fiber configurations. In this mode, the two ends of the fiber flap with large amplitude (Figure 21(b)) like a flapping flag. As the flow velocity increases, the two ends of the fiber combine together and a closed structure can be formed (Figure 21(c)).

During the fluid-flexible fiber interaction process with a relatively shorter fiber length of 3.3 cm [143], two symmetric vortices are generated at two sides of the fiber, and the size of these two vortices increases with the increase of flow velocity. When the flow velocity reaches a certain value, two rows of asymmetric vortices (the so-called Kármán vortex street) are formed, which finally reach a stable state as the flow field is well developed. As for the fluid-flexible structure interactions with a longer flexible fiber, stronger vortices are shed that lead to the flapping of the flexible fiber, and its U shape can no longer be remained, just as shown in Figure 22. In this situation, the bending angle of the violently flapping fiber becomes larger than 90° and sometimes approaches even 180°. It is evident that the SPH-EBG method can well capture different flapping modes of the flexible structure.

The study of vortex shedding influence on the drag of a flexible fiber has drawn attention of many researchers [213,214]. For example, Zhu [214] studied the vortex-introduced vibration of flexible fibers in detail. The large and frequent deformation of fibers result in frequently moving interfaces and a violent interaction between the fluid and the flexible structure that produce great challenges to model the phenomenon numerically. For this, it is an effective idea to implement the coupling of SPH with EGB by allowing the interaction of neighboring fluid and flexible body particles as the SPH and EBG are all particle-based methods. In this way,

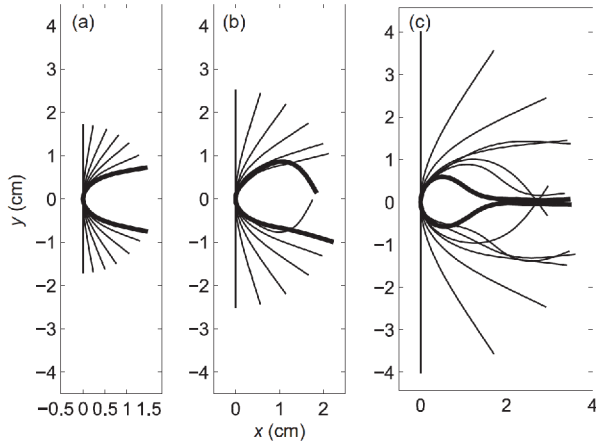

Figure 21 Three typical bending modes of flexible fibers. (a) U-shaped mode (L=3.3 cm), (b) flapping mode (L=5.0 cm), and (c) closed mode (L=8.0 cm).

the SPH-EBG can be regarded as a novel and efficient approach to deal with the fluid-flexible structure interactions.

For modeling the fluid flexible structure interactions, Hu et al. [211,212] coupled the SPH method with the absolute nodal coordinate formulation (ANCF) finite element method, in which the SPH is used to model the fluid flow and ANCF is applied to capture the dynamic response of the flexible bodies. The ANCF, originally proposed by Yakoub and Shabana [215], is an accurate and non-incremental finite element method to deal with the dynamics of a flexible multibody system under both large overall motion and large deformation. Hu et al. [212] applied this coupling method to model the fluid multibody system interactions that involve both the fluid rigid structure and fluid flexible structure interactions. In their works, a rigid double-pendulum is hanged by a flexible cable in air where the double pendulum and flexible cable are modeled by FEM (ANCF for cable) and the air is simulated by using SPH. They studied the trajectories of two points on the rigid double-pendulum with the aerodynamic force considered or not. It can be seen in ref. [212] that the interactions between the fluid and flexible multibody system have much influence on the simulation results, and this problem can only be accurately solved with the fluid-structure interactions considered.

5.4 SPH modeling of FSI problems with granular materials

Fluid-particle interactions or fluid-particle two-phase flows have a wide range of industrial applications including fluidized suspensions, lubrication with transport medium, sedimentation, slurry flow, and food products, etc. In this problem, the granular materials are usually several or large number of particles that have relatively small length scale and low density. Also, due to the small density ratio of granular materials to fluid, the motion of particle is heavily influenced by the surrounding fluid that presents great challenges to the numerical modeling. Thus, the interaction between the fluid and granular materials can be regarded as a special class of FSI problem where the granular materials may be either rigid or deformable. Besides, this problem usually involves a large number of particles, and the interactions between different particles increase the difficulty level in carrying out the simulations.

A lot of numerical techniques have been developed over the past decades for the simulation of this kind of FSI problems [216-219]. As pointed out by Tofighi et al. [220], most of the established fluid-solid simulation methods rely on an

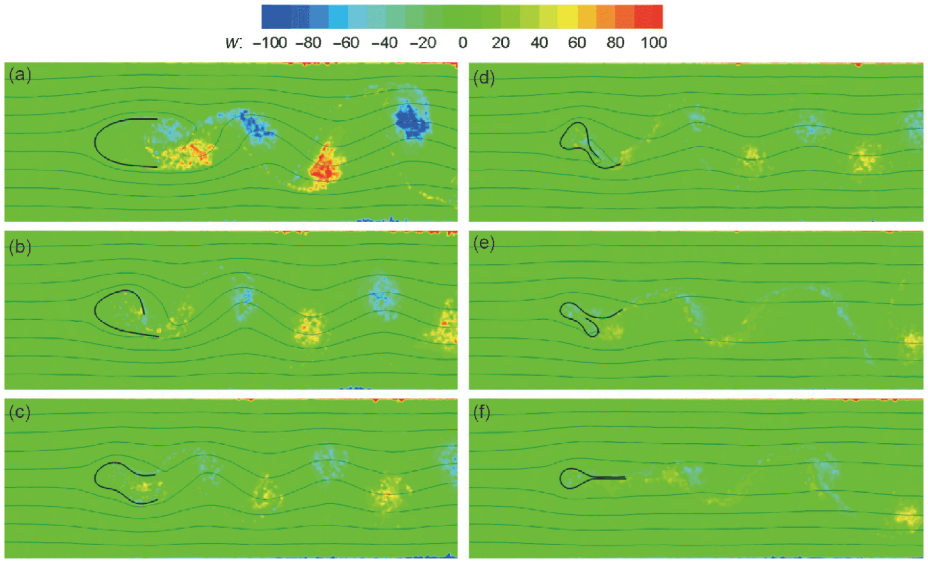

Figure 22 (Color online) The streamlines and vortices of the flexible fiber with length L=8.0 cm at different times (and velocities). The time or flow velocity increases from (a) to (f), with the lines denoting streamlines and the color showing the angular velocity of SPH particles.

underlying fluid mesh that may be moved or refined to adapt the moving boundaries of the solid, which may produce complex algorithms. As a meshfree and particle method, SPH has an inherent advantage over the conventional mesh-based methods as the fluid-solid interaction is realized naturally and the moving boundaries can be traced without additional treatments. However, there are very few articles addressing the application of SPH method to this important class of fluid-structure interaction problem: particulate two-phase flows. Tofighi et al. [220] developed an incompressible SPH (ISPH) method for simulating the motion of rigid bodies in fluids. Hashemi et al. [221] simulated particle sedimentation using a weakly compressible SPH (WCSPH) with modified pressure boundary condition. Bian and Ellero [222] have applied WCSPH to concentrate particle suspensions. Recently, Zhang et al. [80] developed a modified SPH method to effectively simulate fluid-particle interaction problems. The modified SPH includes an enhanced particle approximation scheme, an effective solid boundary treatment algorithm, the artificial stress model and a turbulence model. Here we firstly simulate two sedimentation cases using the modified SPH method and the finite element fictitious boundary method (FE-FBM) [27,29,223] for the sake of making a comparison, i.e., single particle sedimentation (SPS) and dual particle sedimentation (DPS). Figures 23 and 24 show the vertical and horizontal velocity distributions at one time instant in SPS and DPS, respectively. It is noted that the legend magnitude of FE-FBM figures (with unit cm) should be 100 times that of SPH figures (with unit m) due to the unit difference. It is seen that the results obtained using the modified SPH are in good agreements with those from the FE-FBM simulation including the smoothed horizontal and vertical velocity fields, the position and velocity of the settling particle during the sedimentation process. In contrast, the velocity field produced by conventional SPH is very rough, and the positions of two particles also show much deviation from the FE-FBM results.

Figure 25 shows the comparisons of the vertical positions and vertical velocities of two particles, from which we can see that the modified SPH results agree quantitatively with the reference ones [220,224]. The settling velocities obtained from different approaches are expected to have some differences due to the complex physics after the tumbling stage of two particles [225]. For the particle sedimentation problems, the artificial stress is also useful in the modified SPH. It can be seen in Figure 26 that SPH points close to the upper solid boundary obtained without using artificial stress model aggregate together every two or three points, which is a typical stress instability phenomenon. In contrast, with the employment of the artificial stress model, the SPH points distribute more uniformly without evident stress instability, and the simulations in this situation are more accurate and stable.

Furthermore, Zhang et al. [226] developed a finite particle method with particle shifting technique (FPM-PST) to investigate the fluid-particle interaction induced by thermal convection. It is highlighted that this may be the first attempt on the numerical simulation of thermal particulate flows using SPH. The FPM-PST achieves higher accuracy and stability simultaneously, and it can implement the simulation at a higher Rayleigh number by avoiding the possible numerical voids. One may refer to ref. [226] for more details about this method.

In the thermal particulate flow case, a hot particle begins to move in the fluid driven by the gravity and buoyancy force induced by the thermal convection (see the model set-up in ref. [226]). Figure 27 shows the temperature field of the fluid during the particle sedimentation process obtained using FPM-PST and FE-FBM respectively. As shown in Figure 28, the uniform distribution of FPM points and smooth temperature field in the fluid are achieved due to an effective utilization of PST. Figure 29 shows the position and velocity of the settling particle obtained using the FPM-PST and FE-

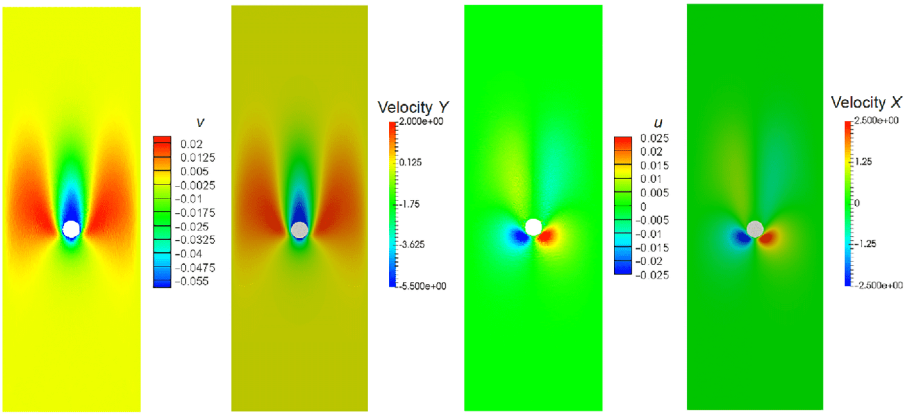

Figure 23 (Color online) Vertical (the first and second columns) and horizontal (the third and fourth columns) velocity distributions at one time instant of single particle sedimentation. The first and third columns are obtained using the modified SPH, and the second and fourth columns are obtained using the FE-FBM.

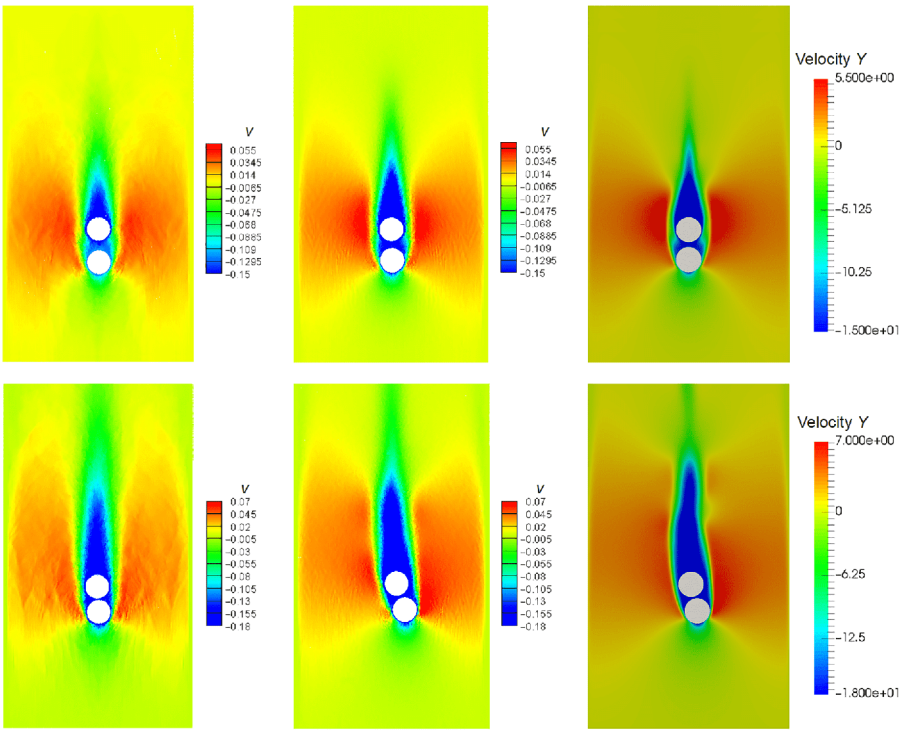

Figure 24 (Color online) Vertical velocity distribution at the dimensionless sedimentation time up: T=10 and down: T=16, obtained using the conventional SPH (left), modified SPH (middle) and FE-FBM (right).

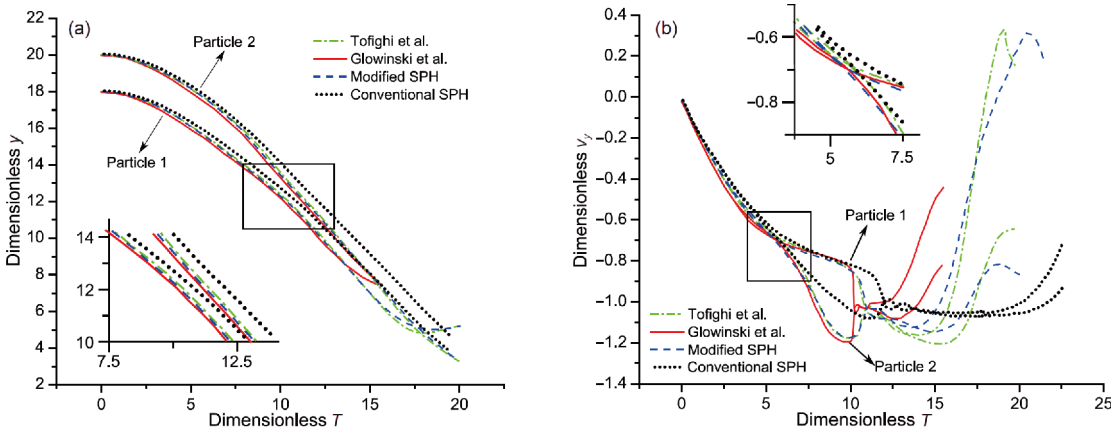

Figure 25 (Color online) Comparison of vertical positions (a) and vertical velocities (b) of two falling particles in a closed channel.

FBM. When the point spacing decreases from L/150 to L/250 or L/350, the results from the FPM-PST simulation get much closer to those from the FE-FBM solutions. It is therefore concluded that FPM-PST can reproduce the settling process of the particle while accurately capturing the heat transfer between the moving particle and the fluid.

5.5 SPH modeling of FSI problems with extremely intensive loadings

In this section, we demonstrate the application of SPH method in modeling impact and explosion problems, which can be regarded as a special type of FSI problems with extremely intensive loadings. The impact and explosion are very important in military and industrial applications. These relevant phenomena tend to complete in a very short duration, when complex chemical reactions and physical processes (e.g., explosive explosion and its driving or damage effects on structures) take place. It is very difficult to study these highly complex processes through an analytical approach since the strong nonlinear fluid and solid dynamics are involved in this problem. Besides, experimental investigations are capable of capturing the explosion and impact phenomenon, but it is difficult for experimental

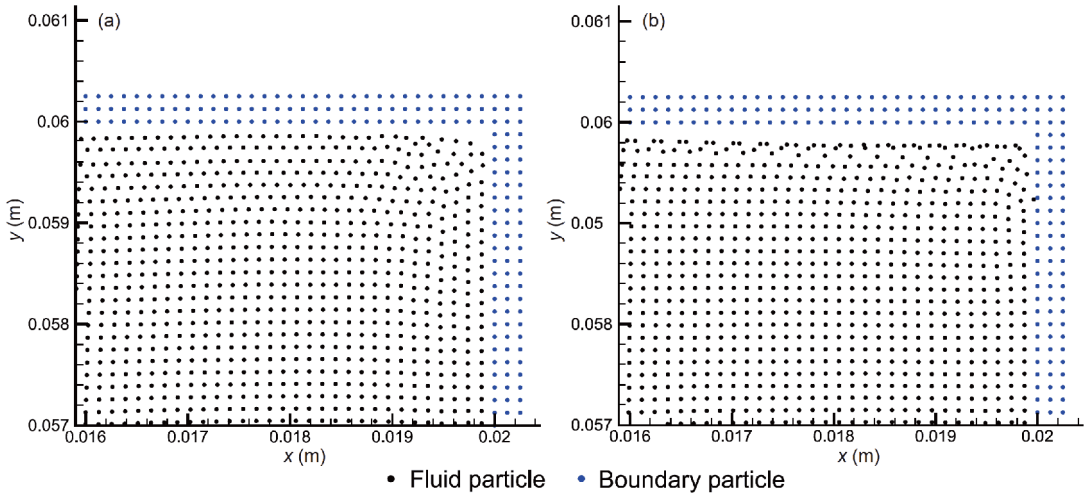

Figure 26 (Color online) Distribution of the SPH points close to the upper solid boundary obtained using present SPH with (a) and without (b) artificial stress model.

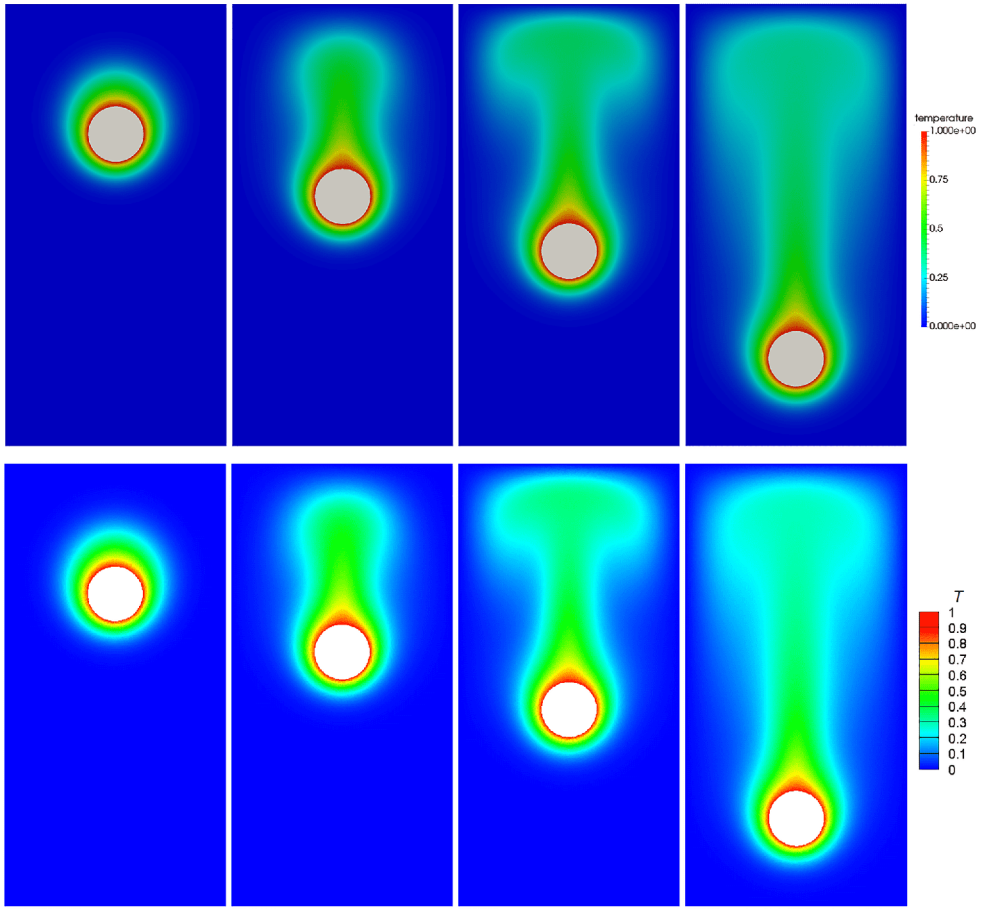

Figure 27 (Color online) Temperature field of the fluid at sedimentation time t=0.2, 0.6, 1.0 and 1.8 s obtained using FE-FBM (a) and FPM-PST (b) respectively, Grashof number Gr=1000.

approach to describe detail information during the explosion process. Recently, more researchers tend to numerically study such problem because the numerical simulation can effectively produce instant observation with considerable reductions in the cost. However, modeling the explosion problem is numerically challenging due to the existence of violent explosion process, strong FSI between the explosive gas and the structures, and extremely large deformations of

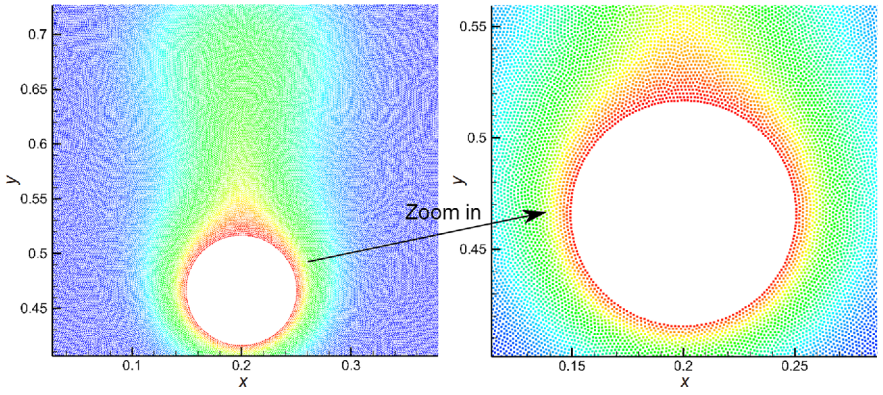

Figure 28 (Color online) Zoom in view of the temperature distribution at sedimentation time 0.6 s obtained using FPM-PST.

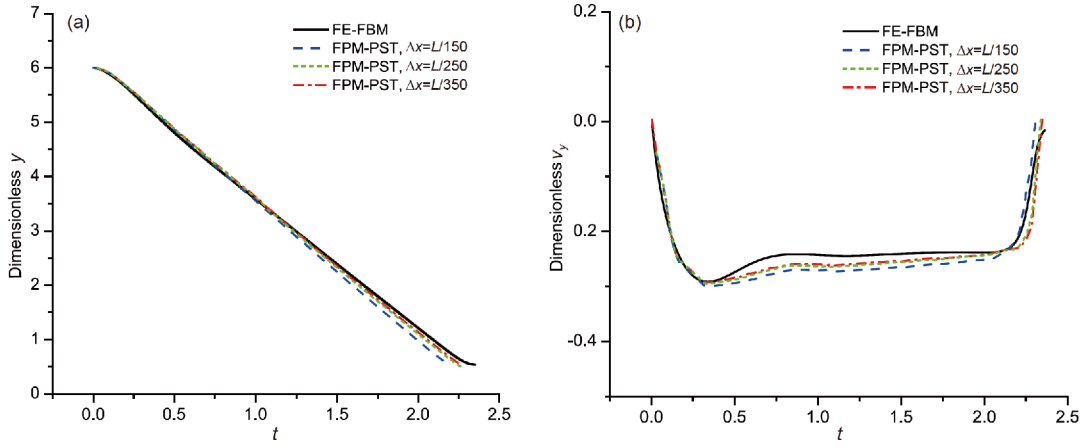

Figure 29 (Color online) Position (a) and velocity (b) of the settling particle obtained using FE-FBM and FPM-PST with different special resolutions, Gr=1000.

structures with even phase changes. The SPH method allows a straightforward handling of FSI with large density ratio (explosive gas to structure) as the connectivity between particles are generated as part of the computation and can change with time. Since its invention, SPH has been successfully applied to model FSI in explosion problems, such as underwater explosion, explosive forming and shaped charge problems [121,123,124,227].

Explosive welding (EXW) is a typical FSI problem with large density ratio between explosive gas and metal plates. In EXW, the flyer plate is driven by the explosion of explosive to impact onto the base plate at a high velocity. In this process, the two plates can be effectively welded together. In most of the existing numerical models, however, the process of EXW is simplified as the impact of two plates while ignoring the explosion process due to the difficulty in effectively modeling the interactions between explosive gas and metal plates. The simplified model is usually referred to as high velocity impact welding (HVIW). At present, there are very few reports considering the driven effects of explosion in EXW [228,229], while some important characteristics of EXW such as the wavy interface and the jetting were not well captured by these approaches.

Recently, Liu et al. [121,128] developed a density-adaptive SPH and successfully applied it to model explosive welding (EXW). In this work, the strong interactions between the explosive gas and the mental plates were effectively modeled, and the typical characteristics of EXW have also been accurately captured, i.e., the explosion wave, wavy interface and jetting formation shown in Figure 30. The wave formation at the material interface is usually an important sign of a successful explosive welding. The SPH simulation results correspond well with the widely accepted wave formation mechanism, i.e., the vortex shedding mechanism [230,231], in which the formation of wavy interface is somewhat similar to the formation of von Kármán vortex street produced by a viscos flow over an obstacle at high Reynolds numbers. It can be seen in the experiments [231] that the interfacial morphology in EXW varies from straight to wavy and then to wavy with vortex shedding as the collision velocity increases (shown in Figure 31(a)-(c)). As shown in Figures 31 and 32, the simulations by adaptive SPH

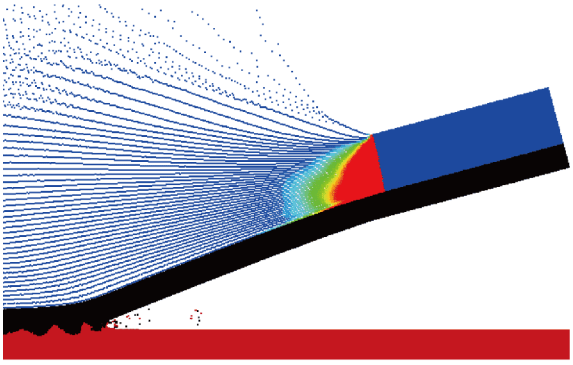

Figure 30 (Color online) A typical snapshot in EXW process obtained by the density-adaptive SPH. The red, black and blue particles represent the base plate, flyer plate and explosive, respectively. The nephogram in explosive represents the explosion wave.

can well reproduce this evolution of the interfacial morphology, and the produced vortices are very similar to the form of von Kármán vortex street.

According to the Vortex Shedding Mechanism, the critical Reynolds number ($R_{\text{transition}}$) is defined to determine the transition of straight to wavy interfacial morphology in EXW,

$$R_{\text{transition}} = \frac{(\rho_{\text{flyer}} + \rho_{\text{base}})V_{\text{c}}^2}{2(H_{\text{flyer}} + H_{\text{base}})}, \tag{56}$$

where R denotes the Reynolds number, ρ and H represent the density (kg/m^3) and Vicker's hardness (N/m^2), respectively. V_{c} (m/s) represents the flow velocity of the flyer material into the collision point. For the steel-steel welding, when the transition of the interfacial morphology occurs, the V_{c} given by eq. (56) is 1960 m/s. The V_{c} obtained from SPH simulation is around 2100 m/s at transition situation of the interfacial morphology (see ref. [128]), which corresponds well with the reference result.

Besides the structure motion driven by an explosion, the penetration of a metal jet on a target due to explosion is also a typical FSI phenomenon. The shaped charges are commonly used in military for penetrating hardened targets and in industry for cutting metals or rocks. This problem involves strong interactions between the high-speed metal jet flow and structure that leads to a large deformation or even broken of structures. Recently, Feng et al. [124] successfully applied SPH to model the linear shaped charge with jet formation (see numerical model in ref. [124]). Figure 33 shows the shape of the formed aluminum jet obtained by the SPH simulation (without showing the explosive gas), which is close to that obtained by Katayama et al. [232] based on experimental and computational observations.

With the SPH simulations, Feng et al. [124] further examined the influence of a surrounding aluminum case on the

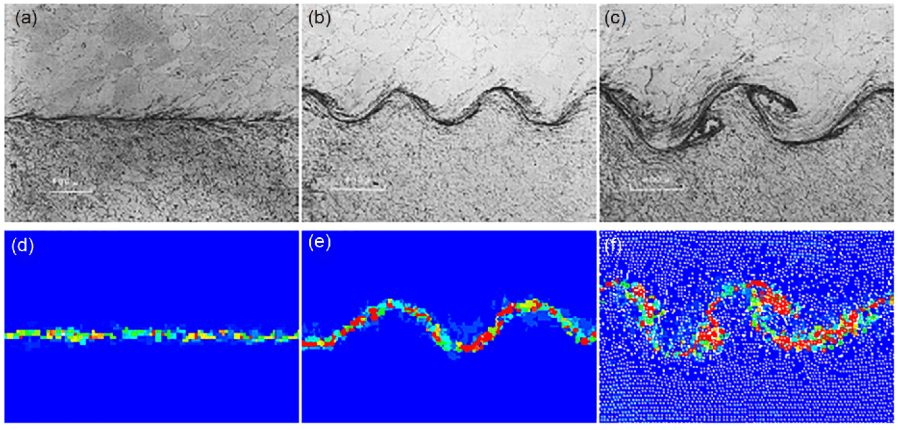

Figure 31 (Color online) Welding interfaces obtained from (a)-(c) experimental observations [231] and (d)-(f) SPH simulations [128].

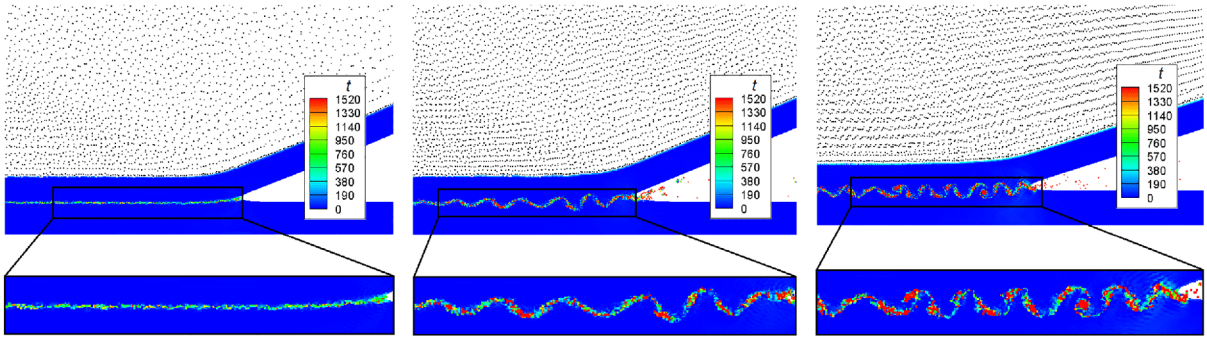

Figure 32 (Color online) Temperature distribution of the flyer and base plates in EXW with increasing amount of explosive from left to right.

shape of the formed metal jet. As shown in Figure 34, the tip of metal jet obtained with surrounding aluminum case is sharper than that obtained without the case. This phenomenon might occur due to the confining effect of the surrounding aluminum case on expansion of the explosive gas. It is thus concluded that the shaped charge with surrounding cases can lead to stronger converging effects with a sharper jet tip. Besides, the penetration effects of the metal jet on a target was also studied based on the SPH simulations. Figure 35 shows the distribution of the metal jet and debris cloud when the aluminum jet penetrates onto a steel plate. It can be clearly seen that the shapes of the hole and debris cloud obtained from the SPH simulation are in qualitatively good accordance with the experimental observations by Raftenberg [233].

6 Concluding remarks

The smoothed particle hydrodynamics (SPH) method is a truly meshfree and Lagrangian particle method which has special advantages over the grid-based methods in treating large deformations and rapidly moving interfaces or free surfaces. Hence, the SPH method and its different variations have been applied to many fluid-structure interaction problems in engineering and sciences. In this, we review the latest developments of SPH in modeling FSI problems. In particular, we introduced in detail the implementation of FSI in the SPH framework and the coupling approaches of SPH with other grid-based or particle-based methods for FSI. The modeling of FSI within a pure SPH framework for both fluids and solids is a monolithic FSI simulation in which the equations governing the fluid flow and the movement of the structure are solved simultaneously with a single SPH solver. In contrast, the modeling of FSI using the coupled approaches is a partitioned FSI simulation in which SPH is applied in the fluid area while the other method is used separately in the structure region. In principle, FSI modeling within a pure SPH framework is more rigorous and straightforward while the representation of moving material interface with virtual particles together with the implementation of interface conditions sometimes can be challenging. FSI modeling with coupled approaches can leverage the advantages of the SPH method and the other coupled method while this weak coupling may lead to delayed interaction and an accurate and robust interface coupling algorithm is necessary.

We also showed SPH modeling of diversified FSI problems including FSI problems with rigid, elastic and flexible structures, FSI problems with granular material and FSI problems with extremely intensive loadings. From the demonstrated FSI examples, we conclude that the SPH method is attractive and has great potential in modeling FSI.

Despite its successful application in modeling FSI problems, SPH is still under development and there are many important numerical aspects that need further investigation.

6.1 Remarks on accuracy, stability and efficiency

The conventional SPH method is infamous for its lower

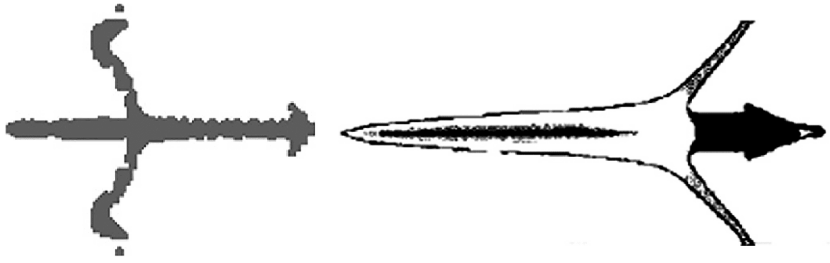

Figure 33 Shape of aluminum jet given by the SPH simulation [124] (a) and reference results [232] (b).

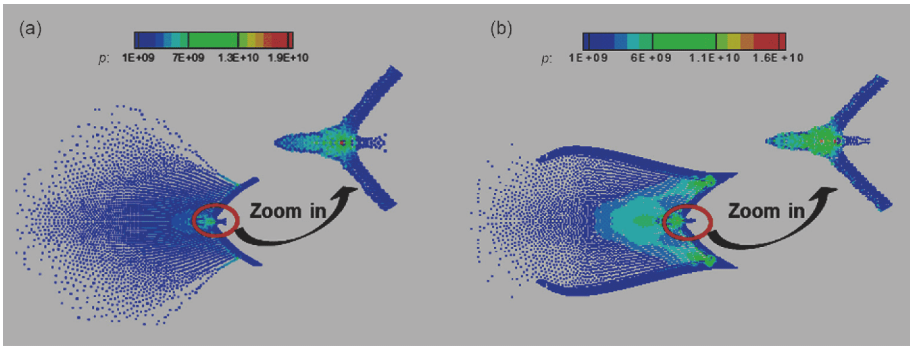

Figure 34 (Color online) Shapes of the formed aluminum jets without (a) and with (b) surrounding aluminum case obtained by SPH simulations.

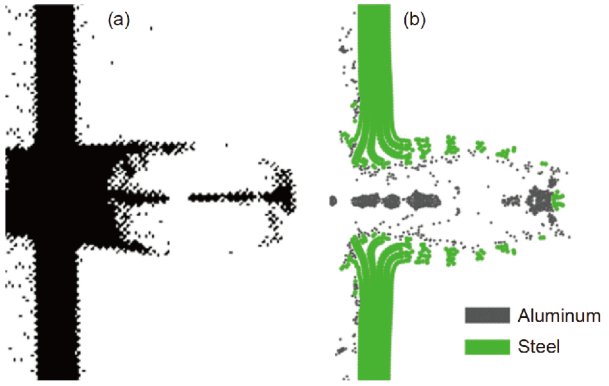

Figure 35 (Color online) Comparison of the experimental radiophoto [233] (a) with the SPH simulation results (b) for the penetration process of a shaped charge.

accuracy and this motivates the development of improved SPH approximation schemes including FPM, CSPM, KGC, KGF-SPH and DFPM, as introduced in sect. 2.2. These modified SPH approximation schemes in general originate from the Taylor series analysis of the SPH approximation of a field function and its derivatives, and a pointwise corrective matrix is used to restore particle consistency and so as to improve the approximation accuracy. However, these approaches put more emphases on the consistency (hence hopefully accuracy), but the stability sometimes can be in question. For example, for FSI problems with singular particle distributions, these methods may suffer from ill-conditioned corrective matrices, which may further lead to numerical instability or unexpected termination of the simulation. Moreover, a pointwise corrective matrix means more computational effort than the conventional SPH that is already computationally expensive compared to grid-based methods. Hence, though the modified SPH approximation schemes are more accurate, they are also less efficient and more unstable.

The question is that can we have the accuracy, stability and efficiency at the same time? The answer is yes, and the DFPM is such a solution. As an improved SPH method, DFPM has much better accuracy while keeping the advantages of flexibility, cost-effectiveness and easiness in computer programming. As a decoupled FPM, DFPM avoids the trouble-some matrix inversion and is more stable and efficient while possessing similar accuracy. Hence, DFPM leverages the high accuracy of FPM and the stability and efficiency of the conventional SPH, and it should be appealing in modeling FSI problems.

6.2 Remarks on FSI interface treatment

As mentioned early, the key challenge in modeling FSI problems is the algorithm to implement the fluid-structure interaction, and the FSI interface algorithms are closely related to the accuracy and applicability of the whole program. When modeling FSI problems with SPH, either in a pure SPH framework as monolithic approach or coupled with other grid- or particle-based methods as partitioned approach, the FSI interface algorithm needs further development. As SPH employs particles to represent the state of the system while the particles move according to internal and external forces, the detection of the interface and the implementation of the interface condition are not as straightforward as that in the grid-based methods. It is natural to treat neighboring particles from different materials as virtual particles which can be used for particle approximation of a concerned interface particle, and this treatment avoids the particle insufficiency problem due to the truncation of the support domain of the particle by the FSI interface. It is also preferable to use the modified SPH approximation schemes on virtual particles for improving the simulation accuracy at the FSI interface.

One important issue is to use a penalty repulsive force to prevent fluid particles from unphysically penetrating solid particles. Though there are some reported repulsive force models, a decent repulsive force should be sufficiently large so as to prevent unphysical particle penetration and should be small enough so that the force will not seriously disturb the bulky flow dynamics. Hence, a robust and versatile repulsive force model can be attractive and is still under development. The other issue is the restoration of the FSI interface consistency, e.g., the consistency of displacement, velocity and stress. So far, the implementation of the FSI interface condition in SPH modeling is not well studied, especially for FSI problems with large density discontinuity, just the same as in SPH modeling of multiphase flows with large density ratios. Hence, some existing algorithms in SPH modeling of multiphase flows including the treatment of large density ratio and the consistency restoring approaches for stress (pressure) can be extendable to SPH modeling of FSI problems. Considering the aforementioned factors, a good choice to implement FSI interface can be the coupled dynamics solid boundary treatment integrated with DFPM approximation and consistency treatment arising from multiphase flows.

6.3 Remarks on coupling of SPH with other methods

As a meshfree Lagrangian particle method, SPH can naturally track moving features and easily treat large deformations, and therefore it is attractive in modeling fluid flows with free surfaces and moving interfaces, in modeling solid dynamics with large deformations, and in modeling FSI problems. Though SPH has developed rapidly in recent years, the balance of accuracy, stability and efficiency is still not fully resolved. Boundary (fixed or movable solid boundary, free surface, moving interface or open boundary) treatment is not as straightforward and accurate as grid-based

methods. Modeling FSI problems in a pure SPH framework as a monolithic approach also need further developments.

In view of the advantages and drawbacks of the SPH method, it is natural to consider combining SPH with other methods to leverage the advantages of each method in suitable region. That is why SPH coupling models are hot in the latest decade, and SPH has been combined with other grid-based (FEM and FVM) and particle-based (DEM and EBG) methods for different FSI problems as partitioned coupling approaches. These coupling approaches are successful to some extent and for some problems, but not omnipotent for diversified applications. So far, as the earliest coupling approach, SPH coupling with FEM (SPH-FEM) is the most studied and most successful. However, even for SPH-FEM, the interaction between SPH particles and FEM elements together with the information exchange still need further study in terms of accuracy, flexibility and robustness. Moreover, the conservations of mass, momentum and even energy should also be seriously considered. It is noted that for SPH modeling of FSI problems, both the monolithic approach in a pure SPH framework and the partitioned approach coupling with other methods undergo development. The competition of these two approaches can surely produces new algorithms for specific or general applications, just as the competition of the particle-based methods with the grid-based methods for modeling FSI problems.

6.4 Particle regularization and adaptive particle resolution

When modeling FSI problems with a grid-based CFD solver for fluids and a grid-based CSD solver for structures, the mesh around the FSI interface needs to be carefully treated and a body-fitted mesh with adaptive mesh refinement is usually preferred. For SPH modeling of FSI problems, the situation is more complicated. Particle regularization and multiresolution can be very attractive, especially around the FSI interface area.

Firstly, the accuracy of the SPH particle approximation is closely related to the deployment of particles. Apart from using higher order SPH approximation schemes as discussed in sect. 2, one other approach is the particle regularization technique, i.e., re-distributing the irregular particles to make them more uniform for better accuracy. During the history of SPH development, different particle regularization techniques including XSPH [55], tensile correction [234], dynamics stabilization [235] and particle shifting techniques [236,237] have been proposed and they can be helpful in modeling complex FSI problems especially for irregular particle distributions. It is important to note that these particle regularization techniques may not be valid for every circumstance. For example, the XSPH may generate unphysical solutions of the viscosity, especially at high velocity gradients or with coarse particle resolution. The tensile correction can somewhat alleviate the tensile instability, but it does not work well in regularizing disordered particles compared to the particle shifting technique. The particle shifting technique may not be very effective for alleviating the tensile instability at high Reynolds numbers, and too much shifting can influence the simulation accuracy. The particle regularization technique may also produce unphysical results at the interface areas for modeling complex FSI problems. Therefore, new particle regularization techniques that could balance the accuracy and stability seem very attractive. Further developments on particle regularization techniques may need to consider the applicability for some complex FSI problems, i.e., FSI at high Reynolds numbers, FSI with breaking free surfaces, and FSI with strong discontinuities at the materials interface.

Secondly, as the particle distribution with equal spacing may not capture important physics around the interface area and the distribution of very refined particles in the whole domain requires prohibitive computational cost, particle distributions with multi-resolutions at different areas or the so-called adaptive particle resolution (APR) are usually necessary. For example, Chiron et al. [99] simulated the water entry of a flat panel with the adaptive particle resolution, in which the interaction region of flat panel and fluid is modeled with very refined particles to accurately capture the local phenomenon. Omidvar et al. [238] model the wave-structure interaction using a simplified multiresolution approach. In their work, a square refined region is used around the cylinder to obtain accurate flow configuration and wave loading on structure.

The very early investigation on adaptivity of SPH was presented in solving astrophysical problems in which a density criterion is used to determine the variation of particle resolution [239]. Feldman and Bonet [100] first proposed a particle refinement technique in which the particles are split into children particles to locally increase the particle resolutions. For particle coarsening, one approach is to merge the children particles passing through the splitting domain into mother particles again. Another coarsening technique is that the mother particle split in a certain region is not removed but switch off and they are turned on after passing through the interested region. Though the APR techniques show some advantages in modeling FSI, there is still a long way to go before APR techniques become as mature as AMR techniques in grid-based methods. One challenge is to maintain the mass, momentum and energy conservation of the particle system during the particle splitting and coarsening process that may affect the simulation accuracy and stability. Also the coarsening stage usually requires expensive computational cost, and more efficient coarsening techniques can be attractive. Besides, using multiresolution in multi-thread systems like GPU remains a big challenge to

be solved. In multi-thread systems such as GPU, the complex load balancing schemes may be required to deal with the memory management problems. At present, there are still limited studies on this technique while the multiresolution in multi-thread systems is very important for application of SPH in industries.

This work was supported by the National Natural Science Foundation of China (Grant No. 51779003), and the National Key Research and Development Project of China (Grant No. 2018YFB0704000). The authors appreciate the help from Dr. Muhammad Saif Ullah Khalid for smoothing the paper and giving constructive suggestions.

1 M. B. Liu, J. R. Shao, and H. Q. Li, Int. J. Numer. Meth. Fluids **74**, 684 (2014).
2 F. R. Ming, A. M. Zhang, H. Cheng, and P. N. Sun, Ocean Eng. **165**, 336 (2016).
3 J. R. Wright, and J. E. Cooper, *Introduction to Aircraft Aeroelasticity and Loads* (Wiley, Weinheim, 2007).
4 W. Shen, and Y. P. Zhao, J. Appl. Mech. **85**, 031003 (2018).
5 M. B. Liu, and G. R. Liu, Arch. Comput. Methods Eng. **17**, 25 (2010).
6 H.-J. Bungartz, *Fluid-structure Interaction: Modelling, Simulation, Optimization* (Springer-Verlag, Heidelberg, 2006).
7 J. F. Sigrist, *Fluid-Structure Interaction: An Introduction to Finite Element Coupling* (Wiley, Weinheim, 2015).
8 Y. C. Fung, *An Introduction to the Theory of Aeroelasticity* (John Wiley & Sons, Ltd., Hoboken, 1994).
9 M. B. Liu, and G. R. Liu, *Particle Methods for Multi-Scale and Multi-Physics* (World Scientific, Singapore, 2016).
10 M. Matsumoto, H. Shirato, T. Yagi, R. Shijo, A. Eguchi, and H. Tamaki, J. Wind Eng. Ind. Aerod. **91**, 1547 (2003).
11 J. R. Shao, H. Q. Li, G. R. Liu, and M. B. Liu, Comput. Struct. **100-101**, 18 (2012).
12 M. Luo, C. G. Koh, and W. Bai, Ocean Eng. **120**, 52 (2016).
13 H. J.-P. Morand, and R. Ohayon, *Fluid-Structure Interaction: Applied Numerical Methods* (Wiley, Weinheim, 1995).
14 E. H. Dowell, and K. C. Hall, Annu. Rev. Fluid Mech. **33**, 445 (2001).
15 W. Shyy, H. S. Udaykumar, M. M. Rao, and R. W. Smith, *Computational Fluid Dynamics with Moving Boundaries* (Dover Publications, New York, 2007).
16 G. Hou, J. Wang, and A. Layton, Commun. Commut. Phys. **12**, 337 (2012).
17 G. R. Liu, and M. B. Liu, *Smoothed Particle Hydrodynamics: A Meshfree Particle Method* (World Scientific, Singapore, 2003).
18 P. Brandimarte, *Finite-Difference Methods for Partial Differential Equations* (Wiley, Weinheim, 1960).
19 T. Liszka, and J. Orkisz, Comput. Struct. **11**, 83 (1980).
20 T. N. Narasimhan, and P. A. Witherspoon, Water Resour. Res. **12**, 57 (1976).
21 J. Kim, D. Kim, and H. Choi, J. Comput. Phys. **171**, 132 (2001).
22 I. Demirdzic, and M. Peric, Int. J. Numer. Meth. Fluids **10**, 771 (1990).
23 P. Jenny, S. H. Lee, and H. A. Tchelepi, J. Comput. Phys. **187**, 47 (2003).
24 G. Strang, G. J. Fix, and D. S. Griffin, J. Appl. Mech. **41**, 62 (1974).
25 J. R. Cho, and H. W. Lee, Comput. Methods Appl. Mech. Eng. **193**, 2581 (2004).
26 S. Mitra, P. P. Upadhyay, and K. P. Sinhamahapatra, Int. J. Numer. Meth. Fluids **56**, 1625 (2008).
27 K. Walayat, Z. Zhang, K. Usman, J. Chang, and M. Liu, Phys. Fluids **30**, 103301 (2018).
28 D. Wan, and S. Turek, Int. J. Numer. Meth. Fluids **51**, 531 (2006).
29 D. Wan, and S. Turek, J. Comput. Appl. Math. **203**, 561 (2007).
30 O. C. Zienkiewicz, and R. L. Taylor, *The Finite Element Method* (McGraw-Hill, New York, 2000).
31 D. Liu, and P. Lin, J. Comput. Phys. **227**, 3921 (2008).
32 A. E. P. Veldman, J. Gerrits, R. Luppes, J. A. Helder, and J. P. B. Vreeburg, J. Comput. Phys. **224**, 82 (2007).
33 C. W. Hirt, and B. D. Nichols, J. Comput. Phys. **39**, 201 (1981).
34 M. Sussman, P. Smereka, and S. Osher, J. Comput. Phys. **114**, 146 (1994).
35 D. Peng, B. Merriman, S. Osher, H. Zhao, and M. Kang, J. Comput. Phys. **155**, 410 (1999).
36 C. Farhat, and M. Lesoinne, Comput. Methods Appl. Mech. Eng. **182**, 499 (2000).
37 M. Souli, A. Ouahsine, and L. Lewin, Comput. Methods Appl. Mech. Eng. **190**, 659 (2000).
38 K. J. Bathe, and H. Zhang, Comput. Struct. **87**, 604 (2009).
39 O. M. Faltinsen, and A. N. Timokha, J. Fluid Mech. **665**, 457 (2010).
40 M. A. Noorian, R. D. Firouz-Abadi, and H. Haddadpour, Int. J. Numer. Meth. Engng. **89**, 1652 (2012).
41 G. Fourey, C. Hermange, D. Le Touzé, and G. Oger, Comput. Phys. Commun. **217**, 66 (2017).
42 A. W. Vreman, J. Fluid Mech. **796**, 40 (2016).
43 A. W. Vreman, *A Staggered Overset Grid Method for Resolved Simulation of Incompressible Flow Around Moving Spheres* (Academic Press Professional, Inc., New York, 2017).
44 W. K. Liu, Y. Chen, S. Jun, J. S. Chen, T. Belytschko, C. Pan, R. A. Uras, and C. T. Chang, Arch. Comput. Methods Eng. **3**, 3 (1996).
45 S. F. Li, and W. K. Liu, Appl. Mech. Rev. **55**, 1 (2002).
46 G. R. Liu, and Y. T. Gu, *An Introduction to Meshfree Methods and Their Programming* (Springer, Heidelberg, 2005).
47 R. A. Gingold, and J. J. Monaghan, Mon. Not. R. Astron. Soc. **181**, 375 (1977).
48 L. B. Lucy, Astron. J. **82**, 1013 (1977).
49 J. J. Monaghan, Annu. Rev. Fluid Mech. **44**, 323 (2012).
50 S. Koshizuka, and Y. Oka, Nucl. Sci. Eng. **123**, 421 (1996).
51 S. Koshizuka, Comput. Fluid Dyn. J. **4**, 29 (1995).
52 S. Shao, C. Ji, D. I. Graham, D. E. Reeve, P. W. James, and A. J. Chadwick, Coast. Eng. **53**, 723 (2006).
53 Z. Chen, Z. Zong, M. B. Liu, and H. T. Li, Int. J. Numer. Meth. Fluids **73**, 813 (2013).
54 A. J. Chorin, Math. Comp. **22**, 745 (1968).
55 J. J. Monaghan, Annu. Rev. Astron. Astrophys. **30**, 543 (1992).
56 A. Zhang, P. Sun, F. Ming, and A. Colagrossi, J. Hydrodyn. **29**, 187 (2017).
57 D. Violeau, and B. D. Rogers, J. Hydraul. Res. **254**, 1 (2016).
58 H. Gotoh, and A. Khayyer, Coast. Eng. J. **60**, 79 (2018).
59 M. S. Shadloo, G. Oger, and D. Le Touzé, Comput. Fluids **136**, 11 (2016).
60 Z. B. Wang, R. Chen, H. Wang, Q. Liao, X. Zhu, and S. Z. Li, Appl. Math. Model. **40**, 9625 (2016).
61 J. J. Monaghan, J. Comput. Phys. **110**, 399 (1994).
62 M. B. Liu, G. R. Liu, K. Y. Lam, and Z. Zong, Comput. Mech. **30**, 106 (2003).
63 L. D. Libersky, A. G. Petschek, T. C. Carney, J. R. Hipp, and F. A. Allahdadi, J. Comput. Phys. **109**, 67 (1993).
64 X. Y. Hu, and N. A. Adams, J. Comput. Phys. **227**, 264 (2007).
65 A. Colagrossi, and M. Landrini, J. Comput. Phys. **191**, 448 (2003).
66 R. A. Dalrymple, and B. D. Rogers, Coast. Eng. **53**, 141 (2006).
67 S. Shao, and E. Y. M. Lo, Adv. Water Res. **26**, 787 (2003).
68 Z. L. Zhang, D. L. Feng, T. Ma, and M. B. Liu, Eng. Anal. Bound. Elem. **98**, 110 (2019).
69 A. Zhang, P. Sun, and F. Ming, Comput. Methods Appl. Mech. Eng. **294**, 189 (2015).
70 J. K. Chen, and J. E. Beraun, Comput. Methods Appl. Mech. Eng. **190**, 225 (2000).
71 M. B. Liu, and G. R. Liu, Appl. Numer. Math. **56**, 19 (2006).
72 M. B. Liu, W. P. Xie, and G. R. Liu, Appl. Math. Model. **29**, 1252

(2005).
73 R. C. Batra, and G. M. Zhang, J. Comput. Phys. **201**, 172 (2004).
74 G. M. Zhang, and R. C. Batra, Comput. Mech. **34**, 137 (2004).
75 J. Fang, R. G. Owens, L. Tacher, and A. Parriaux, J. Non-Newton. Fluid Mech. **139**, 68 (2006).
76 J. Fang, and A. Parriaux, J. Comput. Phys. **227**, 8894 (2008).
77 D. Asprone, F. Auricchio, and A. Reali, Int. J. Numer. Meth. Fluids **65**, 1376 (2011).
78 D. Asprone, F. Auricchio, A. Montanino, and A. Reali, Int. J. Numer. Meth. Eng. **99**, 1 (2014).
79 Z. L. Zhang, and M. B. Liu, Appl. Math. Model. **60**, 606 (2018).
80 Z. L. Zhang, K. Walayat, J. Z. Chang, and M. B. Liu, Int. J. Numer. Meth. Eng. **116**, 530 (2018).
81 C. Huang, J. M. Lei, M. B. Liu, and X. Y. Peng, Int. J. Numer. Meth. Fluids **78**, 691 (2015).
82 C. Huang, J. M. Lei, M. B. Liu, and X. Y. Peng, Int. J. Numer. Meth. Fluids **81**, 377 (2016).
83 J. Ren, T. Jiang, W. Lu, and G. Li, Comput. Phys. Commun. **205**, 87 (2016).
84 G. Oger, D. Le Touzé, D. Guibert, M. de Leffe, J. Biddiscombe, J. Soumagne, and J. G. Piccinali, Comput. Phys. Commun. **200**, 1 (2016).
85 A. Ferrari, M. Dumbser, E. F. Toro, and A. Armanini, Comput. Fluids **38**, 1203 (2009).
86 A. Zhang, X. Cao, F. Ming, and Z. F. Zhang, Appl. Ocean Res. **42**, 24 (2013).
87 H. Wen, B. Ren, P. Dong, and Y. Wang, Appl. Ocean Res. **59**, 366 (2016).
88 J. L. Cercos-Pita, Comput. Phys. Commun. **192**, 295 (2015).
89 Q. Xiong, B. Li, and J. Xu, Comput. Phys. Commun. **184**, 1701 (2013).
90 D. Winkler, M. Meister, M. Rezavand, and W. Rauch, Comput. Phys. Commun. **213**, 165 (2017).
91 S. M. Longshaw, and B. D. Rogers, Adv. Eng. Softw. **83**, 31 (2015).
92 S. Børve, M. Omang, and J. Trulsen, J. Comput. Phys. **208**, 345 (2005).
93 G. Oger, M. Doring, B. Alessandrini, and P. Ferrant, J. Comput. Phys. **213**, 803 (2006).
94 R. Vacondio, B. D. Rogers, P. K. Stansby, and P. Mignosa, Adv. Water Res. **58**, 10 (2013).
95 R. Vacondio, B. D. Rogers, P. K. Stansby, P. Mignosa, and J. Feldman, Comput. Methods Appl. Mech. Eng. **256**, 132 (2013).
96 R. Vacondio, B. D. Rogers, and P. K. Stansby, Int. J. Numer. Meth. Fluids **69**, 1377 (2012).
97 D. A. Barcarolo, D. Le Touzé, G. Oger, and F. de Vuyst, J. Comput. Phys. **273**, 640 (2014).
98 P. N. Sun, A. Colagrossi, S. Marrone, and A. M. Zhang, Comput. Methods Appl. Mech. Eng. **315**, 25 (2017).
99 L. Chiron, G. Oger, M. de Leffe, and D. Le Touzé, J. Comput. Phys. **354**, 552 (2018).
100 J. Feldman, and J. Bonet, Int. J. Numer. Meth. Eng. **72**, 295 (2007).
101 Y. R. López, D. Roose, and C. Recarey Morfa, Comput. Mech. **51**, 731 (2013).
102 S. Koshizuka, A. Nobe, and Y. Oka, Int. J. Numer. Meth. Fluids **26**, 751 (1998).
103 E. S. Lee, C. Moulinec, R. Xu, D. Violeau, D. Laurence, and P. Stansby, J. Comput. Phys. **227**, 8417 (2008).
104 A. Khayyer, H. Gotoh, and S. D. Shao, Coast. Eng. **55**, 236 (2008).
105 H. Gotoh, A. Khayyer, H. Ikari, T. Arikawa, and K. Shimosako, Appl. Ocean Res. **46**, 104 (2008).
106 A. Skillen, S. Lind, P. K. Stansby, and B. D. Rogers, Comput. Methods Appl. Mech. Eng. **265**, 163 (2013).
107 M. Antuono, A. Colagrossi, S. Marrone, and D. Molteni, Comput. Phys. Commun. **181**, 532 (2010).
108 M. Antuono, A. Colagrossi, and S. Marrone, Comput. Phys. Commun. **183**, 2570 (2012).
109 J. P. Vila, Math. Model. Methods Appl. Sci. **9**, 161 (1999).
110 S. I. Inutsuka, J. Comput. Phys. **179**, 238 (2002).
111 J. J. Monaghan, J. Comput. Phys. **136**, 298 (1997).
112 P. Omidvar, P. K. Stansby, and B. D. Rogers, Int. J. Numer. Meth. Fluids **72**, 427 (2013).
113 P. K. Koukouvinis, J. S. Anagnostopoulos, and D. E. Papantonis, Int. J. Numer. Meth. Fluids **71**, 1152 (2013).
114 L. Han, and X. Hu, J. Hydrodyn. **30**, 62 (2018).
115 A. Rafiee, and K. P. Thiagarajan, Comput. Methods Appl. Mech. Eng. **198**, 2785 (2009).
116 M. Liu, J. Shao, and H. Li, J. Hydrodyn. **25**, 673 (2013).
117 F. R. Ming, A. M. Zhang, and X. Y. Cao, Acta Mech. Sin. **29**, 241 (2013).
118 F. R. Ming, A. M. Zhang, and S. P. Wang, Int. J. Appl. Mech. **07**, 1550032 (2015).
119 V. Mehra, and S. Chaturvedi, J. Comput. Phys. **212**, 318 (2006).
120 A. M. Zhang, W. S. Yang, and X. L. Yao, Appl. Ocean Res. **34**, 10 (2012).
121 M. B. Liu, Z. L. Zhang, and D. L. Feng, Comput. Mech. **60**, 513 (2017).
122 P. W. Randles, and L. D. Libersky, Comput. Methods Appl. Mech. Eng. **139**, 375 (1996).
123 M. B. Liu, G. R. Liu, Z. Zong, and K. Y. Lam, Comput. Fluids **32**, 305 (2003).
124 D. L. Feng, M. B. Liu, H. Q. Li, and G. R. Liu, Comput. Fluids **86**, 77 (2013).
125 M. B. Liu, G. R. Liu, K. Y. Lam, and Z. Zong, Shock Waves **12**, 509 (2003).
126 M. B. Liu, G. R. Liu, and K. Y. Lam, Shock Waves **15**, 21 (2006).
127 Z. L. Zhang, and M. B. Liu, Eng. Anal. Bound. Elem. **83**, 141 (2017).
128 Z. L. Zhang, D. L. Feng, and M. B. Liu, J. Manuf. Proc. **35**, 169 (2018).
129 Z. L. Zhang, T. Ma, M. B. Liu, and D. Feng, Int. J. Comput. Methods **16**, 1846001 (2019).
130 A. Zhang, W. S. Yang, C. Huang, and F. Ming, Comput. Fluids **71**, 169 (2013).
131 F. R. Ming, A. M. Zhang, Y. Z. Xue, and S. P. Wang, Ocean Eng. **117**, 359 (2016).
132 P. Wang, A. M. Zhang, F. Ming, P. Sun, and H. Cheng, J. Fluid Mech. **860**, 81 (2019).
133 S. Marrone, A. Di Mascio, and D. Le Touzé, J. Comput. Phys. **310**, 161 (2016).
134 L. Chiron, S. Marrone, A. Di Mascio, and D. Le Touzé, J. Comput. Phys. **364**, 111 (2018).
135 D. Hu, T. Long, Y. Xiao, X. Han, and Y. Gu, Comput. Methods Appl. Mech. Eng. **276**, 266 (2014).
136 T. Long, D. Hu, D. Wan, C. Zhuang, and G. Yang, J. Comput. Phys. **350**, 166 (2017).
137 Z. Li, J. Leduc, J. Nunez-Ramirez, A. Combescure, and J. C. Marongiu, Comput. Mech. **55**, 697 (2015).
138 Q. Yang, V. Jones, and L. McCue, Ocean Eng. **55**, 136 (2012).
139 K. Wu, D. Yang, and N. Wright, Comput. Struct. **177**, 141 (2016).
140 L. C. Qiu, Ind. Eng. Chem. Res. **52**, 11313 (2013).
141 Y. Tang, Q. Jiang, and C. Zhou, Appl. Math. Model. **62**, 436 (2018).
142 X. Yang, and M. Liu, Commun. Comput. Phys. **22**, 1015 (2017).
143 X. Yang, M. Liu, and S. Peng, Phys. Rev. E **90**, 063011 (2014).
144 X. Yang, M. Liu, S. Peng, and C. Huang, Coast. Eng. **108**, 56 (2016).
145 J. J. Monaghan, and J. C. Lattanzio, Astron. Astrophys. **149**, 135 (1985).
146 A. Colagrossi, M. Antuono, and D. Le Touzé, Phys. Rev. E **79**, 056701 (2009).
147 Z. L. Zhang, T. Ma, D. L. Feng, and M. B. Liu, Int. J. Comput. Methods **15**, 1844004 (2018).
148 J. D. Anderson, *Computational Fluid Dynamics: The Basics With Applications* (McGraw Hill, New York, 2002).
149 H. U. Mair, Shock Vib. **6**, 81 (1999).
150 R. Car, and M. Parrinello, Phys. Rev. Lett. **55**, 2471 (1985).
151 H. J. C. Berendsen, J. P. M. Postma, W. F. van Gunsteren, A. DiNola,

and J. R. Haak, J. Chem. Phys. **81**, 3684 (1984).
152 S. Yamamoto, Y. Maruyama, and S. Hyodo, J. Chem. Phys. **116**, 5842 (2002).
153 R. D. Groot, and P. B. Warren, J. Chem. Phys. **107**, 4423 (1997).
154 M. S. Shadloo, A. Zainali, M. Yildiz, and A. Suleman, Int. J. Numer. Meth. Eng. **89**, 939 (2012).
155 D. H. Zhang, Y. X. Shi, C. Huang, Y. L. Si, and W. Li, J. Mar. Sci. Technol. **24**, 73 (2019).
156 P. N. Sun, A. Colagrossi, S. Marrone, M. Antuono, and A. M. Zhang, Comput. Phys. Commun. **224**, 63 (2018).
157 F. Macia, M. Antuono, L. M. Gonzalez, and A. Colagrossi, Prog. Theor. Phys. **125**, 1091 (2011).
158 S. Adami, X. Y. Hu, and N. A. Adams, J. Comput. Phys. **231**, 7057 (2012).
159 J. J. Monaghan, and J. B. Kajtar, Comput. Phys. Commun. **180**, 1811 (2009).
160 B. D. Rogers, and R. A. Dalrymple, *SPH Modeling of Tsunami Waves* (World scientific, Singapore, 2008).
161 S. Kulasegaram, J. Bonet, R. W. Lewis, and M. Profit, Comput. Mech. **33**, 316 (2004).
162 M. Ferrand, D. R. Laurence, B. D. Rogers, D. Violeau, and C. Kassiotis, Int. J. Numer. Meth. Fluids **71**, 446 (2013).
163 A. Amicarelli, G. Agate, and R. Guandalini, Int. J. Numer. Meth. Eng. **95**, 419 (2013).
164 A. Leroy, D. Violeau, M. Ferrand, and C. Kassiotis, J. Comput. Phys. **261**, 106 (2014).
165 Z. Chen, Z. Zong, M. B. Liu, L. Zou, H. T. Li, and C. Shu, J. Comput. Phys. **283**, 169 (2015).
166 S. Adami, X. Y. Hu, and N. A. Adams, J. Comput. Phys. **229**, 5011 (2010).
167 N. Grenier, M. Antuono, A. Colagrossi, D. Le Touzé, and B. Alessandrini, J. Comput. Phys. **228**, 8380 (2009).
168 T. Belytschko, Y. Krongauz, J. Dolbow, and C. Gerlach, Int. J. Numer. Meth. Eng. **43**, 785 (2015).
169 M. B. Liu, J. R. Shao, and J. Z. Chang, Sci. China Technol. Sci. **55**, 244 (2012).
170 Z. Li, J. Leduc, A. Combescure, and F. Leboeuf, Comput. Fluids **103**, 6 (2014).
171 G. Fourey , G. Oger, D. Touzé, and B. Alessandrini, in *IOP Conference Series: Materials Science and Engineering 10* (IOP Publishing, Bristol, 2010), p. 012041.
172 P. H. L. Groenenboom, and B. K. Cartwright, J. Hydraul. Res. **48**, 61 (2010).
173 T. Belytschko, W. K. Liu, and B. Moran, *Nonlinear Finite Elements for Continua and Structures* (John Wiley & Sons Inc., Hoboken, 2014).
174 S. W. Attaway, M. W. Heinstein, and J. W. Swegle, Nucl. Eng. Des. **150**, 199 (1994).
175 Z. Zhang, H. Qiang, and W. Gao, Eng. Struct. **33**, 255 (2011).
176 T. De Vuyst, R. Vignjevic, and J. C. Campbell, Int. J. Impact Eng. **31**, 1054 (2005).
177 E. A. Fadlun, R. Verzicco, P. Orlandi, and J. Mohd-Yusof, J. Comput. Phys. **161**, 35 (2000).
178 R. Mittal, and G. Iaccarino, Annu. Rev. Fluid Mech. **37**, 239 (2005).
179 M. Neuhauser, and J.-C. Marongiu, in *Proceedings of 9th SPHERIC International Workshop* (SPH European Research Interest Community, Paris, 2014).
180 E. Napoli, M. De Marchis, C. Gianguzzi, B. Milici, and A. Monteleone, Comput. Methods Appl. Mech. Eng. **310**, 674 (2016).
181 F. Chen, H. Qiang, and W. Gao, Comput. Chem. Eng. **77**, 135 (2015).
182 F. Chen, H. Qiang, H. Zhang, and W. Gao, Int. J. Numer. Meth. Eng. **109**, 73 (2017).
183 D. Zhou, and R. H. Wagoner, J. Mater. Proc. Tech. **50**, 1 (1995).
184 K.-I. Tsubota, S. Wada, and T. Yamaguchi, J. Mater. Proc. Technol. **1**, 159 (2006).
185 S. M. Hosseini, and J. J. Feng, Chem. Eng. Sci. **64**, 4488 (2009).
186 P. W. Cleary, Miner. Eng. **73**, 85 (2015).
187 B. Ren, Z. Jin, R. Gao, Y. Wang, and Z. Xu, J. Waterw. Port Coast. Ocean Eng. **140**, 04014022 (2014).
188 M. Robinson, M. Ramaioli, and S. Luding, Int. J. Multiphase Flow **59**, 121 (2014).
189 A. M. Zhang, F. R. Ming, and S. P. Wang, Appl. Ocean Res. **43**, 223 (2013).
190 K. Gong, S. Shao, H. Liu, B. Wang, and S. K. Tan, J. Fluids Struct. **65**, 155 (2016).
191 X. Liu, H. Xu, S. Shao, and P. Lin, Comput. Fluids **71**, 113 (2013).
192 L. Wang, F. Xu, Y. Yang, and J. Wang, Eng. Anal. Bound. Elem. **100**, 140 (2019).
193 T. Ye, D. Pan, C. Huang, M. Liu, Phys. Fluids **31** (2019).
194 J. Shao, S. Li, Z. Li, and M. Liu, Eng. Comput. **32**, 1172 (2015).
195 H. Akyildız, and U. N. Erdem, Ocean Eng. **33**, 2135 (2006).
196 O. M. Faltinsen, O. F. Rognebakke, I. A. Lukovsky, and A. N. Timokha, J. Fluid Mech. **407**, 201 (2000).
197 M. Greenhow, and S. Moyo, Philos. Trans. R. Soc. London. Ser. A-Math. Phys. Eng. Sci. **355**, 551 (1997).
198 P. Lin, Comput. Fluids **36**, 549 (2007).
199 P. A. Tyvand, and T. Miloh, J. Fluid Mech. **286**, 67 (1995).
200 G. Oger, L. Brosset, P. M. Guilcher, E. Jacquin, J. B. Deuff, and D. L. Touzé, Int. J. Offshore Polar Eng. **20**, 181 (2010).
201 C. Antoci, M. Gallati, and S. Sibilla, Comput. Struct. **85**, 879 (2007).
202 S. C. Hwang, A. Khayyer, H. Gotoh, and J. C. Park, J. Fluids Struct. **50**, 497 (2014).
203 A. Khayyer, H. Gotoh, H. Falahaty, and Y. Shimizu, Comput. Phys. Commun. **232**, 139 (2018).
204 Y. M. Scolan, J. Sound Vib. **277**, 163 (2004).
205 J. C. Liao, D. N. Beal, G. V. Lauder, and M. S. Triantafyllou, Science **302**, 1566 (2003).
206 T. Y. Wu, Annu. Rev. Fluid Mech. **43**, 25 (2011).
207 S. Vogel, J. Exp. Bot. **40**, 941 (1989).
208 F. Gosselin, E. de Langre, and B. A. Machado-Almeida, J. Fluid Mech. **650**, 319 (2010).
209 S. Alben, M. Shelley, and J. Zhang, Nature **420**, 479 (2002).
210 S. Alben, M. Shelley, and J. Zhang, Phys. Fluids **16**, 1694 (2004).
211 W. Hu, Q. Tian, and H. Hu, Nonlin. Dyn. **75**, 653 (2014).
212 W. Hu, Q. Tian, and H. Y. Hu, Sci. China-Phys. Mech. Astron. **61**, 044711 (2018).
213 L. A. Miller, A. Santhanakrishnan, S. Jones, C. Hamlet, K. Mertens, and L. Zhu, J. Exp. Biol. **215**, 2716 (2012).
214 L. Zhu, J. Fluid Mech. **587**, 217 (2007).
215 R. Y. Yakoub, and A. A. Shabana, J. Mech. Des. **123**, 614 (2001).
216 R. Glowinski, T. W. Pan, T. I. Hesla, and D. D. Joseph, Int. J. Multiphase Flow **25**, 755 (1999).
217 B. K. Mishra, and R. K. Rajamani, Appl. Math. Model. **16**, 598 (1992).
218 S. B. Pillapakkam, and P. Singh, J. Comput. Phys. **174**, 552 (2001).
219 G. J. Wagner, S. Ghosal, and W. K. Liu, Int. J. Numer. Meth. Engng. **56**, 1261 (2003).
220 N. Tofighi, M. Ozbulut, A. Rahmat, J. J. Feng, and M. Yildiz, J. Comput. Phys. **297**, 207 (2015).
221 M. R. Hashemi, R. Fatehi, and M. T. Manzari, Int. J. Non-Lin. Mech. **47**, 626 (2012).
222 X. Bian, and M. Ellero, Comput. Phys. Commun. **185**, 53 (2014).
223 S. Turek, D. Wan, and L. S. Rivkind, Lect. Notes Comput. Sci. Eng. **35**, 37 (2003).
224 R. Glowinski, T. W. Pan, T. I. Hesla, D. D. Joseph, and J. Périaux, J. Comput. Phys. **169**, 363 (2001).
225 G. He, G. Jin, and Y. Yang, Annu. Rev. Fluid Mech. **49**, 51 (2017).
226 Z. L. Zhang, K. Walayat, C. Huang, J. Z. Chang, and M. B. Liu, Int. J. Heat Mass Transfer **128**, 1245 (2019).
227 J. W. Swegle, and S. W. Attaway, Comput. Mech. **17**, 151 (1995).
228 Y. Wang, H. G. Beom, M. Sun, and S. Lin, Int. J. Impact Eng. **38**, 51 (2011).
229 S. A. A. A. Mousavi, and S. T. S. Al-Hassani, Mater. Des. **29**, 1 (2008).

230 S. R. Reid, Int. J. Mech. Sci. **16**, 399 (1974).
231 G. R. Cowan, O. R. Bergmann, and A. H. Holtzman, Metall. Mater. Trans. B **2**, 3145 (1971).
232 M. Katayama, A. Takeba, S. Toda, and S. Kibe, Int. J. Impact Eng. **23**, 443 (1999).
233 M. N. Raftenberg, in *Twelfth Army Symposium on Solid Mechanics Proceedings*, Watertown, USA November 4-7, 1991, edited by S. C. Chou (1992).
234 J. J. Monaghan, J. Comput. Phys. **159**, 290 (2000).
235 N. Tsuruta, A. Khayyer, and H. Gotoh, Comput. Fluids **82**, 158 (2013).
236 R. Xu, P. Stansby, and D. Laurence, J. Comput. Phys. **228**, 6703 (2009).
237 S. J. Lind, R. Xu, P. K. Stansby, and B. D. Rogers, J. Comput. Phys. **231**, 1499 (2012).
238 P. Omidvar, P. K. Stansby, and B. D. Rogers, *Wave Body Interaction in 2D Using Smoothed Particle Hydrodynamics (SPH) With Variable Particle Mass* (John Wiley & Sons, Hoboken, 2012).
239 S. Kitsionas, and A. P. Whitworth, Mon. Not. R. Astron. Soc. **330**, 129 (2002).